

***S*-Type and *P*-Type Habitability in Stellar Binary Systems:
A Comprehensive Approach
III. Results for Mars, Earth, and super-Earth Planets**

Zh. Wang (王兆鹏) and M. Cuntz

Department of Physics

University of Texas at Arlington, Arlington, TX 76019-0059;

`zhaopeng.wang@mavs.uta.edu; cuntz@uta.edu`

ABSTRACT

In Paper I and II, a comprehensive approach was utilized for the calculation of *S*-type and *P*-type habitable regions in stellar binary systems for both circular and elliptical orbits of the binary components. It considered a joint constraint including orbital stability and a habitable region for a possible system planet through the stellar radiative energy fluxes (“radiative habitable zone”; RHZ). Specifically, the stellar *S*-type and *P*-type RHZs are calculated based on the solution of a fourth order polynomial. However, in concurrent developments, mostly during 2013 and 2014, important improvements have been made in the computation of stellar habitable zones for single stars based on updated climate models given by R. K. Kopparapu and collaborators. These models entail considerable changes for the inner and outer limits of the stellar habitable zones. Moreover, regarding the habitability limit given by the runaway greenhouse effect, notable disparities were identified between Earth, Mars, and super-Earth planets due to differences in their atmospheric models, thus affecting their potential for habitability. It is the aim of this study to compute *S*-type and *P*-type habitable regions of binaries in response to the updated planetary models. Moreover, our study will also consider improved relationships between effective temperatures, radii, and masses for low-luminosity stars.

Subject headings: astrobiology — binaries: general — celestial mechanics — planetary systems

1. INTRODUCTION

Do habitable zones¹ (HZs) exist only around single stars? The answer is certainly “no”, according to many years of research pursued by different groups. Previous theoretical results about zones of possible habitability for binary (and higher-order) systems have been obtained by, e.g., Eggl et al. (2012, 2013), Kane & Hinkel (2013), Kaltenegger & Haghighipour (2013), Haghighipour & Kaltenegger (2013), Cuntz (2014, 2015), and Bazsó et al. (2017), among others. The main goal of these studies was the identification of stellar binary systems with respect to different types of planetary and stellar configurations. For example, Bazsó et al. (2017) explored the dynamics and habitability in circumstellar planetary systems of previously identified binaries including the consideration of resonance phenomena.

The overall importance of studying stellar binary systems stems from their relatively high frequency (e.g., Duquennoy & Mayor 1991; Patience et al. 2002; Eggenberger et al. 2004; Lada 2006; Raghavan et al. 2006, 2010; Roell et al. 2012). In fact, following those works, the majority of stars, notwithstanding M-type dwarfs, are not single. Additionally, a significant number of binary systems have also been identified to harbor planets. Following Dvorak (1982), there are two kinds of systems. First, planets may orbit one of the binary components; those are said to be in an *S*-type orbit. In those systems the other stellar component is at a notable distance; however, it may act as a perturber — possibly resulting in considerable orbital ramifications. Second, planets may orbit both binary components; those are said to be in *P*-type orbits. In summary, so far close to 100 planet-hosting binary systems have been identified. A survey on planet-hosting exoplanetary systems, with focus on stellar separations of less than 100 au, has been published by Bazsó et al. (2017). Studies about the successful formation of planets in binary systems have been given by, e.g., Kley & Nelson (2012), Thebault & Haghighipour (2015), and references therein.

In Paper I and II of this series, Cuntz (2014, 2015) focused on a theoretical identification (i.e., ab-initio approach) of *S*-type and *P*-type HZs in binary systems, including the possibility of no HZ after all. The approach-as-elected included (1) the consideration of a joint constraint including orbital stability and a habitable region for a possible system planet through the stellar radiative energy fluxes needs to be met; (2) the treatment of different types of HZs; and (3) the provision of a combined formalism for the assessment of both *S*-type and *P*-type HZs based on the solution of a quartic algebraic equation. Cuntz (2015) presented an expansion of the methodology to binary systems based on elliptical orbits.

A critical aspect pertaining to the calculation of binary HZs is the choice of planetary

¹A glossary of acronyms is given in Appendix A.

climate models. As part of a quasi-contemporaneous development, Kopparapu et al. (2013, 2014) offered new estimates for the widths and extents of HZs around single stars based on significant improvements of the previous work by Kasting et al. (1993). They constructed an updated 1-D radiative–convective, cloud-free climate model based on new data (including, but not limited to, improved H₂O and CO₂ cross sections), which allowed them to calculate revised stellar HZs for F, G, K, and M stars. For one of the climate models, Kopparapu et al. (2014) identified a weak, but nonetheless identifiable, dependency on the planetary mass. In that case, they constructed models appropriate for Mars-type, Earth-type (the previous default), and super-Earth-type planets. This discrepancy has been obtained for the entire set of stars.

In this study we discuss updated results about the structure and existence of HZs in stellar binaries. Our paper is structured as follows. In Section 2, we describe our theoretical approach with focus on the key equations. We also comment on the set of stellar parameters used and on the revised habitable zone estimates. In Section 3, we describe our results and discussion. Our summary and conclusions are given in Section 4.

2. THEORETICAL APPROACH

2.1. Key Equations

The key equations of this study closely follow the previous work given as Paper I and II, and references therein. The habitability limits around single stars can be calculated using

$$d^2 = \frac{L/L_{\odot}}{S_{\text{eff},\ell}} \quad (1)$$

with L/L_{\odot} as the star’s luminosity in units of the solar luminosity, and $S_{\text{eff},\ell}$ as effective stellar flux, in unit of solar constant. The latter is a function of stellar effective temperature, i.e., $S_{\text{eff},\ell} = S_{\text{eff},\ell}(T_{\text{eff}})$ that also depends on the type of HZ limit ℓ (see Section 2.2 for details and discussion. For the Sun itself, the following relationship holds

$$s_{\ell} = S_{\text{eff},\ell}^{-1/2} \quad (2)$$

with s_{ℓ} denoting the various inner/outer limits of the solar HZ.

As focus of our study, we adopt the habitability limits based on the climate models by Kopparapu et al. (2014). They found that the runaway greenhouse effect, readily taken as the inner limit for the general habitable zone (GHZ), also depends on the planetary mass. Thus, we introduce k stands for the type of planet (see Section 2.2). Therefore, we adopt a more generalized notation given as $s_{\ell} \rightarrow s_{\ell k}$ and $S_{\text{eff},\ell} \rightarrow S_{\text{eff},\ell k}$.

Generally, the distinctions between habitability limits of different stars are conveyed through the different choices of stellar luminosity L , effective temperature T_{eff} , type of habitability limit ℓ and planetary mass, if applicable (parameterized through k). In case of (theoretical) main-sequence stars, the number of parameters is further reduced due to the relation between L and T . Interpolations for $S_{\text{eff},\ell k}$ are available; see Appendix B and Figure 2 for details. In the following, we use the approach by Kopparapu et al. (2013, 2014), except if noted otherwise.

For multiple stellar systems with N stars, by taking the radiation from all stellar components into account, the radiative habitable zone (RHZ) — which purposely ignores any orbital stability requirement for possible system planets — can be calculated following the inverse-square law. Hence, the key equation reads

$$\sum_{i=1}^N \frac{L_i/L_{\odot}}{S_{\text{eff},i\ell k} d_i^2} = 1 \quad (3)$$

Akin to Paper I, we define $L'_{i\ell k}$ as

$$L'_{i\ell k} = \frac{L_i}{L_{\odot} S_{\text{eff},i\ell k}} \quad (4)$$

Consequently, the key equation for a binary star system reads

$$\sum_{i=1}^2 \frac{L'_{i\ell k}}{d_i^2} = 1 ; \quad (5)$$

see Figure 1 for information on the system set-up.

The RHZ of the binary system could be found through solving some lengthy algebra (see Paper I and II) involving the solution of a quartic equation²; see Figure 1 for information on the mathematical set-up. Furthermore, the limit of orbital stability needs to be taken into account as well in order to obtain viable stellar HZs, which is done following the work³ by Holman & Wiegert (1999). The orbital stability limit a_{cr} , which depends on the binary

²In Eq. (20) of Paper I, the third term should correctly read $-4A_0y$. However, this typo does not affect any of the calculations in Paper I or subsequent work.

³Updated results for planetary orbital stability concerning both S -type and P -type binary systems have been given by Quarles et al. (2018). However, in those simulations a Jupiter-mass planet has been used as test object to determine the planetary orbital stability limits. Hence, tighter limits have been identified compared to the work by Holman & Wiegert (1999) also used here. However, in the view of the uncertainty bars of the latter work both kinds of results are mutually consistent.

separation a_{bin} , binary eccentricity e_{bin} and stellar masses M_1 and M_2 , is an *upper limit* for *S*-type system centered from the primary star, and a *lower limit* for *P*-type system measured from the binary mass center. Figure 3 depicts a flow diagram on the newly devised online tool **BinHab 2.0** allowing for the computation of the existence of HZs in binary systems. Following the nomenclature of Paper I, if *S*-type and *P*-type HZs are **Truncated** because of the criterion of orbital stability for system planets, the terms *ST*-type and *PT*-type HZs are used.

2.2. Stellar Parameters and Habitable Zone Estimates

For this study, stellar parameters are required for which we adopt standard main-sequence, see, e.g., Baraffe et al. (1998) and Gray (2005). A notable exception, however, are stars of spectral type K and M, for which we consider updated research results; see Table 1 for data on stellar parameters⁴ for stars in the spectral range between F0 and M2. Here we also utilize results by Mann et al. (2013), including their mass – effective temperature and mass – radius relationships as implied. Table 1 conveys the stellar parameters as adopted here ranging from spectral type F0 to M2.

Mann et al. (2013) analyzed moderate resolution spectra for a set of nearby K and M dwarfs with well-known parallaxes and interferometrically determined radii to define their effective temperatures, among other quantities. As part of their efforts, they focused on the hosts of transiting planet candidates in the *Kepler* field to determine the stellar masses and to place additional constraints to the remaining stellar parameters. Generally speaking, for standard (theoretical) main-sequence stars as considered here, the stellar luminosities and masses are closely correlated, which reduces the number of free stellar and system parameters from six (i.e., M_1 , M_2 , L_1 , L_2 , a_{bin} , e_{bin}) to four as the mass and luminosity shall be viewed as mutually redundant. The reason is that for those stars the latter are connected by mass-luminosity relationships; see, e.g., Reid (1987), and references therein. An updated theoretical mass-luminosity relation for K and early M dwarfs has recently been given by Cuntz & Wang (2018).

Another important aspect of our study consists in obtaining adequate HZ estimates. An early version of this concept has been introduced by Kasting et al. (1993) [Kas93]. As

⁴In Paper I and II, the Sun was equated to a theoretical main-sequence stars of $T_{\text{eff}} = 5811$ K following Gray (2005). In the present work, we assume $T_{\text{eff}} = 5780$ K, a value (within its uncertainty bar) identical to the observed value of 5777 K (Stix 2004), as also used in the climatological studies by Kopparapu et al. (2013, 2014).

inner limits of HZs, they used criteria following conditions akin to Recent Venus (RV), the runaway greenhouse effect, and the moist greenhouse effect. As outer limits of HZs, they used criteria following conditions akin to Early Mars (EM), the maximum greenhouse effect (no clouds), and the first CO₂ condensation; Furthermore, following Kasting et al. (1993), the occurrence of the runaway greenhouse effect means that the greenhouse phenomenon is enhanced by water vapor, resulting in surface warming. As indicated by the models, that effect further increases the atmospheric vapor content, leading to an additional rise of the planetary surface temperature.

Furthermore, water loss criterion means that an atmosphere is warm enough to have a wet stratosphere, from where water is gradually lost by atmospheric chemical processes to space. The first CO₂ condensation, a criterion later abandoned by Kopparapu et al. (2013, 2014) [Kop1314], indicates the stellar distance where CO₂ start to form, thus significantly shaping the planetary climate conditions at larger distances as well; see Table 2 for comparisons for habitability limits pertaining to the Sun, s_ℓ , as used by different authors. Regarding the runaway greenhouse limit, Kopparapu et al. (2014) also found a weak, but nonetheless identifiable, dependency on the planetary mass. Their models allowed to calculate limits for Mars-type ($M = 0.1 M_\oplus$), Earth-type ($M = M_\oplus$), and super-Earth-type ($M = 5.0 M_\oplus$) planets considered here as well. Regarding index $\ell = 2$, denoting the limit due to the runaway greenhouse effect (an inner limit), an additional index k is used, with $k = 1, 0, 2$ indicating an Earth-type, Mars-type, or super-Earth-type planet, respectively.

These definitions allow to define the limits for the RVEM, GHZ, as well as conservative habitable zone (CHZ); see Table 3 for details including comparisons with previous work. In Paper I and II, we largely followed the conventions proposed by Kasting et al. (1993), except we did not consider the RVEM HZ. Instead, we utilized the extended habitable zone (EHZ)⁵ introduced by Mischna et al. (2000). The outer limit of the EHZ signifies the maximum greenhouse effect, assuming 100% cloud coverage, based on a simplified model available at the time. It is noteworthy that there are no universally accepted definitions what constitutes the CHZ and GHZ, as those tend to vary from author-to-author. In Table 3, we list the ones adopted by Kopparapu et al. (2013, 2014), as well as those used in the present work where we use the conventions GHZ and RVEM. Furthermore, Table 4 conveys the main target list

⁵ The work by Mischna et al. (2000), not used here, but considered in Paper I and II, has been superseded by more recent studies, including work by Halevy et al. (2009), Pierrehumbert & Gaidos (2011), Kitzmann (2016), and Ramirez & Kaltenecker (2017, 2018). Kitzmann (2016) argued that the heating assumed by Mischna et al. (2000) has been overestimated, thus putting the extension of the outer HZ in question. Pierrehumbert & Gaidos (2011) pointed out that planetary HZs could actually extend to up to 10 AU for solar-like stars. Additional results, including those for methane-based HZs, have been given by Ramirez & Kaltenecker (2017, 2018).

for this study, encompassing stars of masses 1.25, 1.00, 0.75, and $0.50 M_{\odot}$, corresponding to (approximate) spectral types of F8 V, G2 V, K2 V, and M1 V, respectively. Stellar data, i.e., effective temperature T_{eff} and radius R_{*} , are obtained through interpolation for set values of stellar mass. Regarding stellar luminosity, this selection of stars corresponds to a range between $2.15 L_{\odot}$ and $3.59 \times 10^{-2} L_{\odot}$.

The acquisition of updated stellar parameters, based either on theory or observations, is an ongoing process. Especially the derivation of mass-luminosity-radius-spectral type relationships for M-dwarfs has proven to be particularly challenging; for information on current research see, e.g., Veyette et al. (2017) and references therein. Although most of our study utilizes the stellar parameters of Mann et al. (2013), as an example of comparison with other data, we calculate selected models for both P - and S -type habitability for middle M dwarfs based on the data of Baraffe et al. (2015). These authors have provided evolutionary models for pre-main-sequence and main-sequence low-mass stars while utilizing updated data bases. The differences for the HZs as obtained are relatively minor, and are most pronounced for pairs of M-dwarfs; see Section 3.2.3 for details.

2.3. Comments on the Coordinate System

Regarding the coordinate system (COS) used for our study, the semi-distance between the stellar components is also referred to as semi-major axis a . The COS's origin is placed at the center between the two stellar components as previously done in Paper I and II. Observationally, the distance between the stellar components is denoted⁶ as a_{bin} , i.e., relationship

$$a = \frac{1}{2}a_{\text{bin}} . \quad (6)$$

From the perspective of orbital mechanics, it is of interest to consider cases of different mass ratios μ given as

$$\mu = \frac{M_2}{M_1 + M_2} \quad (7)$$

with M_1 and M_2 denoting the mass of the stellar primary (S1) and stellar secondary (S2), respectively. Clearly, both stellar components will orbit about the common center of mass (CM). The distances of S1 and S2 from the CM are denoted as Z and a_{orb} , respectively (see Fig. 4), with a_{orb} given as

$$a_{\text{orb}} = 2a(1 - \mu) \quad (8)$$

⁶Occasionally, especially in observational astronomy, a_{bin} is referred to as semi-major axis as well, which is due to the different choices of the COS.

For equal-mass systems, i.e., $\mu = 1/2$, we find $a_{\text{orb}} = a$, whereas in the limiting case of very small mass for the secondary (e.g., the Sun-Jupiter pair, if treated as a binary), we find $a_{\text{orb}} \simeq 2a$. Information for a_{orb}/a values for systems of different stellar mass ratios, including those considered here, is given in Figure 4.

3. RESULTS AND DISCUSSIONS

3.1. Solution Landscapes

Next we explore the general solution landscape for HZs of stellar binary systems. Additional results pertaining to the widths of HZs, both with respect to the RVEM and GHZ, can be found in Section 3.2. Here we present a limited number of examples, encompassing both equal-mass and non-equal-mass systems, while assuming either $e_{\text{bin}} = 0.0$ or $e_{\text{bin}} = 0.25$. We also discuss the structure and extent of the GHZ for Mars-type ($0.1 M_{\oplus}$), Earth-type ($1.0 M_{\oplus}$), and super-Earth-type planets ($5.0 M_{\oplus}$). Furthermore, we comment on the relationship between the respective RHZ and the orbital stability limit for possible system planets. Results for *P*-type HZs are given in Figures 5 and 6, whereas results for *S*-type HZs are given in Figure 7. Additional results are given in Tables 5 and 6. Generally, orbital stability limits of possible system planets may impede on the zones of habitability. This type of behavior may occur regarding *P*-type and *S*-type HZs. If it does occur, *PT*-type and *ST*-type HZs are obtained, respectively.

Regarding *P*-type HZs, our results, chosen in lieu of similar cases, read as follows: For systems with binary semi-major axes $a_{\text{bin}} = 0.25$ au, *P*-type GHZs can be found for both the $M_1 = M_2 = 1.00 M_{\odot}$ and the $M_1 = 1.00 M_{\odot}$ & $M_2 = 0.50 M_{\odot}$ cases. The outer limit for the equal-mass case ranges⁷ from 2.37 to 2.38 au; thus, the minimum value which is 2.37 au must be taken as outer limit for the RHZ (see Paper I for further discussion). For a Mars-type planet, the GHZ’s inner limit ranges from 1.42 to 1.44 au, for an Earth-type planet, it ranges from 1.34 to 1.36 au, and for a super-Earth-type planet, it ranges from 1.29 to 1.32 au. Here the maximum values must be taken as adequate limits for the RHZs, given as 1.44, 1.36, and 1.32 au, respectively. The orbital stability limit for possible system planets is given as

⁷For the GHZ and RVEM-type limits, as well as the planetary orbital stability limits, values of higher precision than those given here are readily included in Tables 5 to 10. This was done mostly for tutorial reasons; it is known, however, that the limits of stellar HZs and those of orbital stability are inherently uncertain owing to various processes and effects not included in this study. Examples include the particulars of atmospheric compositions, space and planetary weather patterns, and tidal heating; see, e.g., Ramirez (2018) for details.

0.60 au. It is located well inside the inner limit of the RHZ for a Mars-type, Earth-type, or super-Earth-type planet. Therefore, with respect to the GHZ, the full extent of the RHZ is available in each case.

Figure 5 depicts the case of $M_1 = 1.00 M_\odot$ & $M_2 = 0.50 M_\odot$ with $a_{\text{bin}} = 0.25$ au. Here both the outer and inner limits of the RHZs are reduced owing to the lower luminosity of the secondary stellar component. Here the outer limit of the RHZ is given as 1.65 au, whereas the inner limits for the RHZ are given as 1.10, 1.05, and 1.01 au for a Mars-type, Earth-type, and super-Earth-type planet, respectively. The orbital stability limit for possible system planets is given as 0.60 au. It is again located well inside the inner limit of the RHZs for the three cases studied. Therefore, the full extent of the RHZ is again available as GHZ in each case.

In case of $e_{\text{bin}} = 0.25$, there are only minor changes to the systems. The outer limits of the RHZs are reduced, whereas the inner limits of the RHZs are increased. Additionally, the orbital stability limits for possible system planets, both for the equal-mass and the non-equal-mass system, are increased. However, in both cases, the orbital stability limits remain below the limits of the RHZs; therefore the full extents of the RHZs are available as GHZ in each case. However, the situation is considerably changed if systems of larger separations are considered. Table 5 and 6 show some values for the habitability classification, including $e_{\text{bin}} = 0.50$ and 0.75 . In summary, the maximum value of a_{bin} for *P*- or *PT*-type habitability to exist significantly decreases if e_{bin} is increased. Thus, there will be many systems without *P/PT*-type habitability, at least following the approach adopted here.

This result is also exemplified by Figure 6, which is based on $a_{\text{bin}} = 0.50$ au. In this case, for the equal-mass system, the RHZ’s outer limit is given as 2.36 au. Here the inner limits for the RHZ are given as 1.48, 1.40, and 1.37 au for a Mars-type, Earth-type, and super-Earth-type planet, respectively. Here the orbital stability limit for possible system planets is given as 1.19 au, and therefore does not impede on the RHZs. Again, the full extents of the RHZs are available for facilitating habitability regarding the GHZ. However, this situation is drastically different for the non-equal-mass system of $M_1 = 1.00 M_\odot$ & $M_2 = 0.50 M_\odot$, or if the orbital eccentricity is changed to $e_{\text{bin}} = 0.25$.

If we take the equal-mass system with $M_1 = M_2 = 1.00 M_\odot$ with $e_{\text{bin}} = 0.25$ as an example, the RHZ’s outer limit is given as 2.35 au. Here the inner limits for the RHZ are given as 1.52, 1.44, and 1.40 au for a Mars-type, Earth-type, and super-Earth-type planet, respectively, whereas the orbital stability limit for possible system planets is given as 1.53 au. Hence, the orbital stability limit is inside the RHZ for all three cases of possible system planets, and the available HZ is notably reduced (i.e., *PT*-type habitability). Furthermore, in this type of system, the available HZ does not depend on the type of system planet. A more

drastic case is given by the non-equal-mass system with $M_1 = 1.00 M_\odot$ & $M_2 = 0.50 M_\odot$, $a_{\text{bin}} = 0.50$ au, and $e_{\text{bin}} = 0.25$. Here the outer limit of the RHZ varies between 1.57 and 1.91 au, with 1.57 au identified as relevant number. Moreover, the orbital stability limit for possible system planets is given as 1.61 au. Therefore, according to the model adopted in this work, there is no GHZ available in this system.

S-type habitability always occurs if the distance between the stellar components is chosen sufficiently large, noting that the minimum distance increases as a function of the stellar luminosities. Figure 7 explores some examples of *S*-type cases, taking the equal-mass and non-equal-mass systems, as previously discussed, while assuming $a_{\text{bin}} = 5.0$ au as well as $e_{\text{bin}} = 0.0$ or 0.25 . Our calculations show that an *S*-type GHZ is able to exist around the primary star for the non-equal mass case considered here. The RHZ’s outer limit has a minimum of 1.68 au, which is smaller than 1.69 au, the stability limit for possible system planets; here $e_{\text{bin}} = 0.0$ is assumed. The inner limits of the RHZ are 1.01, 0.95, and 0.92 au for a Mars-type, Earth-type, and super-Earth-type planet, respectively. Furthermore, an *ST*-type GHZ is found around the stellar primary for the equal-mass case. The orbital stability limit, given as 1.37 au, is notably smaller than the RHZ’s outer limit, given as 1.73 au; it thus represents the outer limit of GHZ. Here the inner limits pertaining to the Mars-type, Earth-type and super-Earth-type planets are given as 1.04, 0.98, and 0.94 au, respectively.

If larger eccentricities are chosen, changes occur, as expected, but they are much less profound than in the *P*-type case. For $e_{\text{bin}} = 0.25$, the changes in the RHZ limits are very small compared to circular orbit in the non-equal mass system due to the reduced luminosity of the secondary as well as the large separation distance. A major difference, however, arises from the orbital stability limit, which shapes the GHZ, as the outer limit is now identified as 1.17 au. In case of the equal mass system with $e_{\text{bin}} = 0.25$, the outer limit of RHZ changes to 1.71 au. The inner limits of RHZ are identified as 1.09, 1.01, and 0.97 au for the Mars-type, Earth-type, and super-Earth-type planets, respectively. However, no HZ could be found in this case, as the orbital stability limit at 0.96 au is less than the RHZ’s inner limit.

Table 5 and 6 list the limits for *P*-type, *PT*-type, *S*-type, and *ST*-type habitability for different systems regarding both the GHZ and RVEM HZ. It is revealed that higher eccentricities for the system components always entail higher limiting values for a_{bin} pertaining to the *S/ST*-type case. High values of eccentricity mean that the two stellar components will have relatively close approaches at periapsis implying increased impediment, as indicated by the structure of the RHZs and orbital stability limits. Therefore, for highly eccentric stellar orbits, relatively large separation distances are required for *S*-type habitability to be realized. Moreover, increased values of eccentricity also adversely impact *P/PT*-type habitability, but the impact is less severe.

3.2. Widths of Binary Habitable Zones

3.2.1. *P-Type Case Studies*

Next we discuss some examples pertaining to the widths of binary HZs. First, we focus on *P*-type case studies. Results are given in Figures 8, 9, and 10, as well as in Table 7 and 8. The widths are given as a function of eccentricity of the stellar components. Combining the constraints (see Section 2.1), which include (1) the existence of the RHZ (radiative criterion) and (2) the orbital stability limit of possible system planets (gravitational criterion), the width of *P/PT*-type HZs is given as

$$\text{Width (P/PT)} = \text{RHZ}_{\text{out}} - \text{Max}(\text{RHZ}_{\text{in}}, a_{\text{cr}}) \quad (9)$$

where RHZ_{in} and RHZ_{out} denote the inner and outer limit of the RHZ, respectively, and a_{cr} denotes the limit of orbital stability (which is a lower limit). No *P/PT*-type HZ is found if the width following Eq. (9) is less than or equal to zero.

Figures 8, 9, and 10 showcase systems of stars of different masses, with combinations for M_1 and M_2 of 1.25, 1.00, 0.75, and 0.50 M_{\odot} taking into account $a_{\text{bin}} = 0.25$ au and 0.50 au. Regarding the eccentricity of the systems, we assume e_{bin} to take values between 0.0 and 0.80. Note that both RVEM HZs and GHZs are considered. Figure 8 and 9 refer to Earth-type planets; note that a total of 12 combinations of stellar masses are taken into account. In the following, we focus on a limited number of examples aimed at highlighting distinct trends.

For the *P*-type RVEM (see Figure 8), the combination of $M_1 = M_2 = 0.75 M_{\odot}$ with $a_{\text{bin}} = 0.25$ au entails *PT*-type HZs for eccentricities larger than 0.148. For mass combinations of $M_1 = 1.00 M_{\odot}$ & $M_2 = 0.50 M_{\odot}$, the limiting value for the eccentricity is given as 0.348. Furthermore, for mass combinations of $M_1 = 1.00 M_{\odot}$ & $M_2 = 0.75 M_{\odot}$, the respective value for the eccentricity is 0.630. The three other cases depicted in Figure 8 entail *P*-type HZ when the binary eccentricities are less than or equal to 0.80 (the upper limit considered). If the semi-major axis is taken as 0.50 au, the combination of $M_1 = M_2 = 0.75 M_{\odot}$ indicates *PT*-type HZs for eccentricities less than or equal to 0.272. This values reads 0.286 for mass combinations of $M_1 = 1.00 M_{\odot}$ & $M_2 = 0.50 M_{\odot}$, and 0.714 for for mass combinations of $M_1 = 1.00 M_{\odot}$ & $M_2 = 0.75 M_{\odot}$. Cases of *PT*-type HZs are found for $M_1 = M_2 = 1.00 M_{\odot}$ for all eccentricities studied. If the eccentricity is below 0.021, *P*-type HZs exist for $M_1 = 1.25 M_{\odot}$ & $M_2 = 0.50 M_{\odot}$. For mass combinations of $M_1 = 1.25 M_{\odot}$ & $M_2 = 0.75 M_{\odot}$, the limiting eccentricity is identified as 0.058.

Comparing the widths of HZs for the GHZ and different planetary climate models (see Figure 9), the *PT*-type HZs correspond to smaller differences than *P*-type HZs. This result

is as expected, noting that the stellar fluxes of the maximum greenhouse limit from the two models are relatively similar, with both inner limits being set by the orbital stability limit. As only the runaway greenhouse limit depends on the planetary mass, thus potentially affecting the widths of their HZs, Earth-type planets are found to have HZs of smaller widths than super-Earth-type planets, but their HZs are of larger widths than for Mars-type planets in P -type cases. For PT -type cases, those widths are always the same; see Figure 10 for details. Generally speaking, for fixed combinations of stellar masses, an increase in eccentricity reduces the width of P/PT -type HZs in each case. This effect is, however, less pronounced if the separation distance between the stellar binary components is relatively small.

Table 7 depict selected critical values of eccentricities for different stellar mass combinations, i.e., P/PT -type HZs are possible below those values but not at higher eccentricities. Table 7 lists information for a_{bin} of 0.25 au and 0.50 au both with respect to the RVEM and GHZ; for the latter, Earth-type planets are assumed. For $a_{\text{bin}} = 0.25$ au and the GHZ, 9 out of the 10 stellar mass combinations feature either P -type HZs or PT -type HZs, although for some low-mass combinations there is a restriction regarding eccentricity. However, this number is considerably reduced for $a_{\text{bin}} = 0.50$ au or if the RVEM-type HZ is selected. Another finding is, however, that one of the mass combinations falls short. For equal-mass systems of $M_1 = M_2 = 0.50 M_{\odot}$ very small separation distances need to be assumed in order to identify P -type HZs or PT -type HZs. For the GHZ and Earth-type planets, that semi-major axis reads 0.124, 0.096, 0.082, and 0.074 au for P -type HZs and 0.218, 0.212, 0.206, and 0.200 au for PT -type HZs with respect to eccentricities of 0.00, 0.25, 0.50, and 0.75, respectively. Table 8 depicts comparisons between Mars-type, Earth-type, and super-Earth-type planets with respect to the GHZ. No notable differences are found with respect to high-mass combinations, especially concerning small binary separation distances, but for low-mass combinations, planets of lower mass are advantageous for the existence of P -type HZs. However, the orbital stability limit plays a key role in the existence of P/PT -type HZs.

3.2.2. S -Type Case Studies

In the following, we focus on S -type case studies. Results are given in Figures 11, 12, and 13, as well as in Tables 9 and 10. The widths are given as a function of eccentricity of the stellar components. Combining the constraints (see Section 2.1), which include (1) the existence of the RHZ (radiative criterion) and (2) the orbital stability limit of possible system planets (gravitational criterion), the width of S/ST -type HZs is given as

$$\text{Width}(S/ST) = \text{Min}(\text{RHZ}_{\text{out}}, a_{\text{cr}}) - \text{RHZ}_{\text{in}} \quad (10)$$

where RHZ_{in} and RHZ_{out} denote the inner and outer limit of the RHZ, respectively, and a_{cr} denotes the limit of orbital stability (which is an upper limit). No S/ST -type HZ is found if the width following Eq. (10) is less than or equal to zero.

In the following, we focus on the study of S -type RVEM HZs and GHZs based on binary semi-major axes of $a_{\text{bin}} = 10.0$ au and 20.0 au. Our aim is to identify the maximum (i.e., critical) values of the eccentricity for the existence of the HZs. In selected cases, we also explore the differences in the HZs with respect to Mars-type, Earth-type, and super-Earth-type planets. We will focus on the same stellar mass combinations as done for P -type cases, see Section 3.2.1.

Considering S -type RVEM HZs (see Figure 11 and Table 9) for equal-mass systems of $a_{\text{bin}} = 10.0$ au and $M_1 = M_2 = 1.00 M_{\odot}$, $M_1 = M_2 = 0.75 M_{\odot}$, and $M_1 = M_2 = 0.50 M_{\odot}$ the maximum eccentricities for S -type HZs to be able to exist are 0.295, 0.517, and 0.785, respectively. The corresponding values for ST -type HZ are 0.642, 0.754, and at least 0.80 (the maximum value investigated). This means a general increase in the maximal permissible eccentricity for S/ST -type HZs to be able to exist in decreasing order of stellar masses and luminosities. If we consider $a_{\text{bin}} = 20.0$ au instead, the maximum eccentricities for S -type HZs to be able to exist for $M_1 = M_2 = 1.00 M_{\odot}$ and $M_1 = M_2 = 0.75 M_{\odot}$ are given as 0.602 and 0.723, respectively. The corresponding values for ST -type HZ are 0.791 for $M_1 = M_2 = 1.00 M_{\odot}$ and at least 0.80 for the other mass combinations considered in this study.

Furthermore, it is particularly interesting to explore the existence of S -type and ST -type RVEM HZs for the non-equal-mass system of $M_1 = 1.25 M_{\odot}$ & $M_2 = 0.75 M_{\odot}$. Here the sum of the two masses is identical to the $M_1 = M_2 = 1.00 M_{\odot}$ system, but it has a notably higher luminosity (see Table 4). For this non-equal-mass system it is found that for $a_{\text{bin}} = 10.0$ au S -type and ST -type RVEM HZs ease to exist at eccentricities of 0.177 and 0.580, respectively. Moreover, for $a_{\text{bin}} = 20.0$ au S -type and ST -type RVEM HZs ease to exist at eccentricities of 0.529 and 0.755, respectively. Hence, we are able to conclude that, in general, equal-mass systems are advantageous over non-equal-mass systems in providing S -type and ST -type HZs for highly eccentric cases, and so are systems with relatively large separation distances. Table 9 contains additional examples of non-equal-mass systems as, e.g., $M_1 = 1.00 M_{\odot}$ & $M_2 = 0.50 M_{\odot}$, which can be readily compared to the case of $M_1 = M_2 = 0.75 M_{\odot}$. However, this does not necessarily indicate that the width of the RVEM HZs is reduced compared to the corresponding equal-mass system, see Figure 11.

The differences in HZ widths can also be compared between different types of models. In S/ST -type GHZs, the widths are mostly determined by the differences in the stellar fluxes of runaway greenhouse limit (see Figure 12). Note that the outer limit of the GHZ does

not depend on the planetary mass. Therefore, the HZ width of Earth-type planet is always smaller than the one of super-Earth-type planet, and larger than the one that is Mars-type (see Figure 13). Table 9 and 10 depict selected critical values of eccentricities for different stellar mass combinations. In almost all cases, the limiting values for the eccentricity is less than 0.80 to ensure the full availability of S/ST -type habitability. Again, it is found that values for the eccentricity, generally speaking, highest for super-Earth-type planets, followed by Earth-type planets and Mars-type planets. Generally, high values for the eccentricity affect the existence of HZs in S -type cases in an adverse manner. In S -type cases, this phenomenon appears to be more pronounced than in P -type cases. The adverse effect of high eccentricities appears to be more notable regarding RVEM HZs, in considering of the fact that those HZs are, generally speaking, more extended than GHZs.

3.2.3. Comparative Studies based on Data by Baraffe et al. (2015)

In the following, we present results of comparative studies between models involving the data by Mann et al. (2013) and Baraffe et al. (2015). We assume pairs of M-type dwarfs (equal-mass cases) and pairs consisting of an M-dwarf and a star like the Sun (non-equal-mass cases). We consider models for P - and S -type habitability as well as models involving either circular or elliptical orbits. The stellar parameters of the M-type dwarf are given in Table 11. It shows that for the example as selected the luminosity of the M-dwarf based on the data by Baraffe et al. (2015) is reduced by $\sim 20\%$ compared to that based on the data by Mann et al. (2013). Generally, the luminosities of M-dwarfs are very small compared to solar-type stars. Hence, the extents of HZs are significantly reduced, and the positions of the HZs are much closer-in compared to stars of solar-type luminosities. The lower luminosity of the M-dwarf following Baraffe et al. (2015) will further add to this outcome.

Table 12 conveys the results of our study for equal-mass M-type dwarfs. As expected, the widths of the HZs are reduced if the star data of Baraffe et al. (2015) are adopted, and those HZs are positioned closer-in. This behavior is identified for both P - and S -type models, as well as for $e_{\text{bin}} = 0.00$ and 0.40 , as explored. However, those reductions are minor only; they are identified as approximately 10% for all cases studied. Table 13 conveys the results for pairs containing an M-dwarf and a star like the Sun. It is found that the differences between the models based on the Mann et al. (2013) data and the Baraffe et al. (2015) data are highly irrelevant, i.e., on the order of 0.1% or less. In fact, the differences are totally insignificant for the kind of unequal pairs studied here as the more luminous star completely dominates the outcome. If pairs with lesser differences in the luminosities were considered, the expected outcome would be intermediated between the cases of Table 12 and 13.

4. SUMMARY AND CONCLUSIONS

This studies extends the works previously presented in Paper I and II. The underlying mathematical concept follows a comprehensive approach for the computation of HZs in stellar binary systems. This approach is based on (1) the consideration of a joint constraint including orbital stability and a habitable region for a possible system planet through the stellar radiative energy fluxes needs to be met; (2) the treatment of different types of HZs as defined for the Solar System; the latter utilizes previous models of planetary atmospheres around different types of main-sequence stars given by Kopparapu et al. (2013, 2014); (3) the provision of a combined formalism for the assessment of both *S*-type and *P*-type HZs based on detailed mathematical criteria, i.e., akin to previous work mathematical criteria are presented for which kind of system *S*-type and *P*-type habitability is realized; and (4) applications to stellar systems for different masses in either circular or elliptical orbits.

With respect to the planetary climate models, we discuss both the GHZ and RVEM case as defined here and previously used by other authors. Regarding the outer limit for the GHZ, we consider three different limits, pertaining to Mars-type, Earth-type, and super-Earth-type planets, entailing somewhat different limits for the run-away greenhouse effect, as previously discussed by Kopparapu et al. (2014). The associated planetary masses are given as $0.1 M_{\oplus}$, $1.0 M_{\oplus}$, and $5.0 M_{\oplus}$, respectively. Our theoretical simulations focus on stars with fixed masses given as $1.25 M_{\odot}$, $1.00 M_{\odot}$, $0.75 M_{\odot}$, and $0.50 M_{\odot}$, respectively. Special attention should be given to pairs of low-mass stars, i.e., $0.75 M_{\odot}$ and $0.50 M_{\odot}$, considering that the frequency of those stars is significantly higher compared to high-mass stars (including the Sun) as pointed out by, e.g., Kroupa (2001, 2002). Note that the astrophysical potential of those stars has been explored by, e.g., Heller & Armstrong (2014), Kasting et al. (2014), and Cuntz & Guinan (2016).

Regarding the work given in Paper I and II, we confirm the following findings:

- (1) As discussed in Paper I and II, the solution of the underlying quartic equation proves to be a powerful tool to identify *S*-type and *P*-type habitability in stellar binary systems. The cases of *ST*-type and *PT*-type habitability can be identified as well.
- (2) If the stellar system components have a sufficiently large separation, *S/ST*-type habitability is identified. If the separation is sufficiently small, *P/PT*-type habitability is identified; this result is in alignment with previous findings given in the literature.
- (3) Generally, stellar components with relatively high luminosities favor large-widths HZs. However, the HZs are significantly reduced in size (or even eliminated) if the luminosities of the two stellar components are highly unequal. This effect applies to *P/PT*-type HZs, and it is mostly due to the reduction of the respective RHZs.

(4) Concerning the facilitation of habitability, systems of low eccentricity are advantageous compared to systems of high eccentricity. This outcome is due to the different structures of the RHZs as well as the fact that high eccentricities for the stellar components have an adverse impact on planetary orbital stability. Adverse impacts due to high eccentricities are most pronounced for *S/ST*-type HZs. In addition, adverse impacts are most pronounced in systems of low-luminosities stars, i.e., K and M dwarfs.

Our main findings concerning the work of this study includes:

(1) The width of the HZs, identified for the GHZ, is notably increased for super-Earth-type planets, compared to Earth-type and Mars-type planets. The reason is that the GHZ’s inner limit is set by the runaway greenhouse effect, see Kopparapu et al. (2014), which moderately depends on the planet’s mass.

(2) Exceptions regarding (1) are observed for *P*-type cases at high stellar eccentricities. Here the width of the HZs is determined by the orbital stability requirement rather than the inner limits of the RHZs. Therefore, the general results about the widths of the HZs are independent of the type of planet taken into account.

(3) Relatively large widths for the HZs (if existing) are identified for the GHZ in systems of super-Earth-type planets compared to Earth-type planets, and moreover compared to Mars-type planets. This statement particularly applies to systems where the eccentricity of the binary components is small, the luminosities of the binary components are high, or both.

(4) As default, we used the stellar data by Mann et al. (2013); however, we also pursued selected comparative studies based on the data by Baraffe et al. (2015). The differences in the context of this study are mostly insignificant, except that the latter data imply lower luminosities for M dwarfs. Thus, the widths of HZs are slightly reduced for pairs of those kinds of stars, but not for systems containing a high-luminosity component as the impact of the latter is most decisive.

(5) This study also employed updated limits for the HZs as given by Kopparapu et al. (2013, 2014) compared to limits previously available in the literature. The most pronounced difference is found for the GHZ that is significantly reduced. This outcome reveals itself in calculations for the widths of both *P*-type and *S*-type cases.

(6) There are notable differences in the figures on the widths of HZs, displayed as function of e_{bin} , for *S*-type and *P*-type cases conveying the turnoff points; the latter are given by the impact of planetary orbital stability. In *S*-type cases, the orbital stability limit acts as an outer limit for the HZs, which is relevant for large values of e_{bin} , truncating the GHZ for cases with different planetary masses at the same eccentricity. For small values of e_{bin} , the

widths of the HZs are determined by the RHZs, and thus with respect to the GHZ, there are different outcomes for Mars-type, Earth-type, and super-Earth-type planets. In P -type cases, the orbital stability limit acts as an inner limit for the HZs, again relevant for large values of e_{bin} , but that impact is less pronounced. Hence, there are once again differences between Mars-type, Earth-type, and super-Earth-type planets occurring at low values of e_{bin} .

Besides the results described here, there is a serious need for future work, including various theoretical expansions as well as observational verifications with the help of existing and future space missions. A crucial aspect pertains to the consideration of alternate and expanded definitions of planetary habitability. Examples of recent ideas include work by Pierrehumbert & Gaidos (2011), and Ramirez & Kaltenegger (2018) who identified possible extensions of the classical HZ due to hydrogen and methane clouds, respectively. Furthermore, according to previous studies planetary habitability may be able to persist if planets temporarily exit the stellar HZ, and re-enter.

This behavior is particularly relevant for planets with thick atmospheres. In that context, a readily encountered scenario pertains to planets in highly elliptical orbits; see, e.g., Williams & Pollard (2002), Kane & Gelino (2012), and Pilat-Lohinger et al. (2016) for previous work. In this case, owing to the ability of the planetary atmosphere to store energy, the average (or median) amount of stellar radiation seems to matter most rather than the orbit-dependent amounts. Another important future application of our methodology, i.e., the identification of S -type and P -type HZs through a joint formalism should include the exploration of relationships between the existence of those zones and stellar evolution, i.e., the slow but persistent departure of one of the stellar components from the main-sequence. Previous studies outside of the methodology described in this paper series have been given by, e.g., Underwood et al. (2003), Asghari et al. (2004), Jones et al. (2005), Truitt et al. (2015), and Gallet et al. (2017). General aspects and open questions about planets that are also relevant for planets hosted by binary systems have been discussed by, e.g., Kasting & Catling (2003), Lammer et al. (2009), Kaltenegger (2017), Ramirez (2018), among others.

The authors wish to draw the reader’s attention to the online tool **BinHab 2.0**, hosted at The University of Texas at Arlington (UTA), which allows the calculation of habitable regions in binary systems based on the developed method. This tool has been updated in January 2019.

A. GLOSSARY OF ACRONYMS

Acronym *Meaning*

CHZ	Conservative Habitable Zone (see Paper I and II)
COS	Coordinate System
EHZ	Extended Habitable Zone (see Paper I and II)
GHZ	General Habitable Zone
HZ	Habitable Zone
RHZ	Radiative Habitable Zone
RVEM	Recent Venus / Early Mars (Zone)

B. EFFECTIVE STELLAR FLUX APPROXIMATIONS

In the following, we compare various effective stellar flux approximations available in the literature, which are needed for calculating HZ limits for stars of different effective temperatures (see Figure 2). Originally, Kasting et al. (1993) provided stellar fluxes for standard M0, G2, and F0 main-sequence stars with effective temperatures of 3700 K, 5700 K, and 7200 K, respectively. In order to apply their climate model to main-sequence stars of different spectral types, fitting equations are required. Previously, the two most widely used were those of Underwood et al. (2003) and Selsis et al. (2007).

Underwood et al. (2003) adopted a set of parabolic equations to fit the stellar fluxes, in units of solar constant, dependent of the choice of s_ℓ (see Section 2.2), which are given as

$$S_{\text{eff}} = a_y T_{\text{eff}}^2 + b_y T_{\text{eff}} + c_y . \quad (\text{B1})$$

Here T_{eff} denotes the stellar effective temperature; see their text for coefficient data. Selsis et al. (2007) provided another formalism for interpolating the stellar fluxes as also used by Cuntz (2014, 2015); it is considered here as well for comparison. The stellar fluxes, in units of solar constant, read

$$S_{\text{eff}} = (s_\ell - a_x T_{**} - b_x T_{**}^2)^{-2} . \quad (\text{B2})$$

Here s_ℓ represents different HZ limits following Kasting et al. (1993), see Table 2, with $T_{**} = T_{\text{eff}} - 5700$ K. Selsis et al. (2007) also conveys the various coefficients a_x and b_x for the various climate models with boundaries tagged as s_ℓ .

Kopparapu et al. (2013) obtained new results for solar limits of habitability based on their updated climate model, which is a considerably revised version of the one previously given by Kasting et al. (1993) and also used by Wang & Cuntz (2017). This updated 1D radiative convective, cloud-free climate model has new CO₂ and H₂O absorption coefficients, taken from new data bases, a crucial improvement over previous works. Moreover, they use a recast form for the equation of stellar flux calculation given as

$$S_{\text{eff}} = S_{\text{eff}\odot} + aT_* + bT_*^2 + cT_*^3 + dT_*^4 \quad (\text{B3})$$

Here $T_* = T_{\text{eff}} - 5780$ K; see their table 3 for information on the coefficients.

Subsequently, another revision was made by Kopparapu et al. (2014) who also took the planetary mass into account, with detailed consideration of N₂ background pressure. That model considered Mars-type ($0.1 M_\oplus$), Earth-type, and super-Earth-type ($5.0 M_\oplus$) planets — as done as part of our study as well. They found that the runaway greenhouse limit notably depends on the planetary mass. A very weak dependency, though negligible in consideration of the model’s uncertainties, was also identified for the Early Mars limit; thus

it is ignored here as well. Moreover, they also gave some minor updates for some of the other coefficients previously obtained by Kopparapu et al. (2013); see their table 1 for information.

REFERENCES

- Asghari, N., Broeg, C., Carone, L., et al. 2004, *A&A*, 426, 353
- Baraffe, I., Homeier, D., Allard, F., & Chabrier, G. 2015, *A&A*, 577, A42
- Baraffe, I., Chabrier, G., Allard, F., & Hauschildt, P. H. 1998, *A&A*, 337, 403
- Bazsó, Á., Pilat-Lohinger, E., Eggl, S., Funk, B., Bancelin, D., & Rau, G. 2017, *MNRAS*, 466, 1555
- Cuntz, M. 2014, *ApJ*, 780, 14 [Paper I]
- Cuntz, M. 2015, *ApJ*, 798, 101 [Paper II]
- Cuntz, M., & Bruntz, R. 2014, in *Cool Stars, Stellar Systems, and the Sun: 18th Cambridge Workshop*, ed. G. von Belle & H. Harris (Flagstaff: Proc. Lowell Observatory), p. 831
- Cuntz, M., & Guinan, E. F. 2016, *ApJ*, 827, 79
- Cuntz, M., & Wang, Zh. 2018, *RN AAS*, 2a, 19
- Duquennoy, A., & Mayor, M. 1991, *A&A*, 248, 485
- Dvorak, R. 1982, *OAWMN*, 191, 423
- Eggenberger, A., Udry, S., & Mayor, M. 2004, *A&A*, 417, 353
- Eggl, S., Pilat-Lohinger, E., Georgakarakos, N., Gyergyovits, M., & Funk, B. 2012, *ApJ*, 752, 74
- Eggl, S., Haghighipour, N., & Pilat-Lohinger, E. 2013, *ApJ*, 764, 130
- Gallet, F., Charbonnel, C., Amard, L., Brun, S., Palacios, A., & Mathis, S. 2017, *A&A*, 597, A14
- Gray, D. F. 2005, *The Observation and Analysis of Stellar Photospheres*, 2nd edn. (Cambridge: Cambridge University Press)
- Haghighipour, N., & Kaltenegger, L. 2013, *ApJ*, 777, 166
- Halevy, I., Pierrehumbert, R. T., & Schrag, D. P. 2009, *J. Geophys. Res.*, 114, D18112
- Heller, R., & Armstrong, J. 2014, *Astrobiol.*, 14, 50
- Holman, M. J., & Wiegert, P. A. 1999, *AJ*, 117, 621

- Kaltenegger, L., & Haghighipour, N. 2013, *ApJ*, 777, 165
- Jones, B. W., Underwood, D. R., & Sleep, P. N. 2005, *ApJ*, 622, 1091
- Kaltenegger, L. 2017, *ARA&A*, 55, 433
- Kane, S. R., & Gelino, D. M. 2012, *Astrobiol.*, 12, 940
- Kane, S. R., & Hinkel, N. R. 2013, *ApJ*, 762, 7
- Kasting, J. F., & Catling, D. 2003, *ARA&A*, 41, 429
- Kasting, J. F., Whitmire, D. P., & Reynolds, R. T. 1993, *Icarus*, 101, 108
- Kasting, J. F., Kopparapu, R., Ramirez, R. M., & Harman, C. E. 2014, *Proc. Nat. Aca. Sci.*, 111, 12641
- Kitzmann, D. 2016, *ApJ*, 817, L18
- Kley, W., & Nelson, R. P. 2012, *ARA&A*, 50, 211
- Kopparapu, R. K., Ramirez, R., Kasting, J. F., et al. 2013, *ApJ*, 765, 131; Erratum 770, 82
- Kopparapu, R. K., Ramirez, R. M., SchottelKotte, J., et al. 2014, *ApJ*, 787, L29
- Kroupa, P. 2001, *MNRAS*, 322, 231
- Kroupa, P. 2002, *Science*, 295, 82
- Lada, C. J. 2006, *ApJ*, 640, L63
- Lammer, H., Bredehöft, J. H., Coustenis, A., et al. 2009, *A&A Rev.* 17, 181
- Mann, A. W., Gaidos, E., & Ansdell, M. 2013, *ApJ*, 779, 188
- Mischna, M. A., Kasting, J. F., Pavlov, A., & Freedman, R. 2000, *Icarus*, 145, 546
- Patience, J., White, R. J., Ghez, A. M., et al. 2002, *ApJ*, 581, 654
- Pierrehumbert, R., & Gaidos, E. 2011, *ApJ*, 734, L13
- Pilat-Lohinger, E., Lammer, H., Bancelin, D., Erkaev, N. V., Bazsó, Á., & Eggl, S. 2016, in *The Astrophysics of Planetary Habitability*, Poster Paper
- Quarles, B., Satyal, S., Kostov, V., Kaib, N., & Haghighipour, N. 2018, *ApJ*, 856, 150
- Raghavan, D., Henry, T. J., Mason, B. D., et al. 2006, *ApJ*, 646, 523

- Raghavan, D., McAlister, H. A., Henry, T. J., et al. 2010, *ApJS*, 190, 1
- Ramirez, R. M. 2018, *Geosciences*, 8 (8), 280
- Ramirez, R. M., & Kaltenegger, L. 2017, *ApJ*, 837, L4
- Ramirez, R. M., & Kaltenegger, L. 2018, *ApJ*, 858, 72
- Reid, N. 1987, *MNRAS*, 225, 873
- Roell, T., Neuhäuser, R., Seifahrt, A., & Mugrauer, M. 2012, *A&A*, 542, A92
- Selsis, F., Kasting, J. F., Levrard, B., et al. 2007, *A&A*, 476, 1373
- Stix, M. 2004, *The Sun: An Introduction*, 2nd edn. (A&A Library, Berlin: Springer)
- Thebault, P., & Haghighipour, N. 2015, in *Planetary Exploration and Science: Recent Results and Advances*, ed. S. Jin, N. Haghighipour, & W.-H. Ip (Springer International Geophysics), p. 309
- Truitt, A., Young, P. A., Spacek, A., Probst, L., & Dietrich, J. 2015, *ApJ*, 804, 145
- Underwood, D. R., Jones, B. W., & Sleep, P. N. 2003, *IJAsB*, 2, 289
- Veyette, M. J., Muirhead, P. S., Mann, A. W., Brewer, J. M., Allard, F., & Homeier, D. 2017, *ApJ*, 851, 26
- Wang, Zh., & Cuntz, M. 2017, *AJ*, 154, 157
- Williams, D. M., & Pollard, D. 2002, *IJAsB*, 1, 61

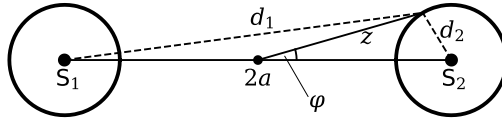
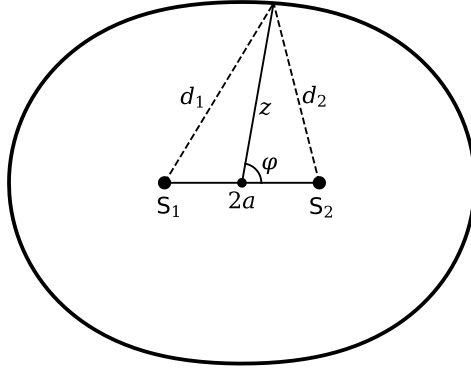


Fig. 1.— Set-up for the mathematical treatment of P -type (top) and S -type (bottom) habitable zones of binary systems as given by the stellar radiative fluxes with $a \equiv \frac{1}{2}a_{\text{bin}}$. Note that the stars S_1 and S_2 have been depicted as identical for convenience.

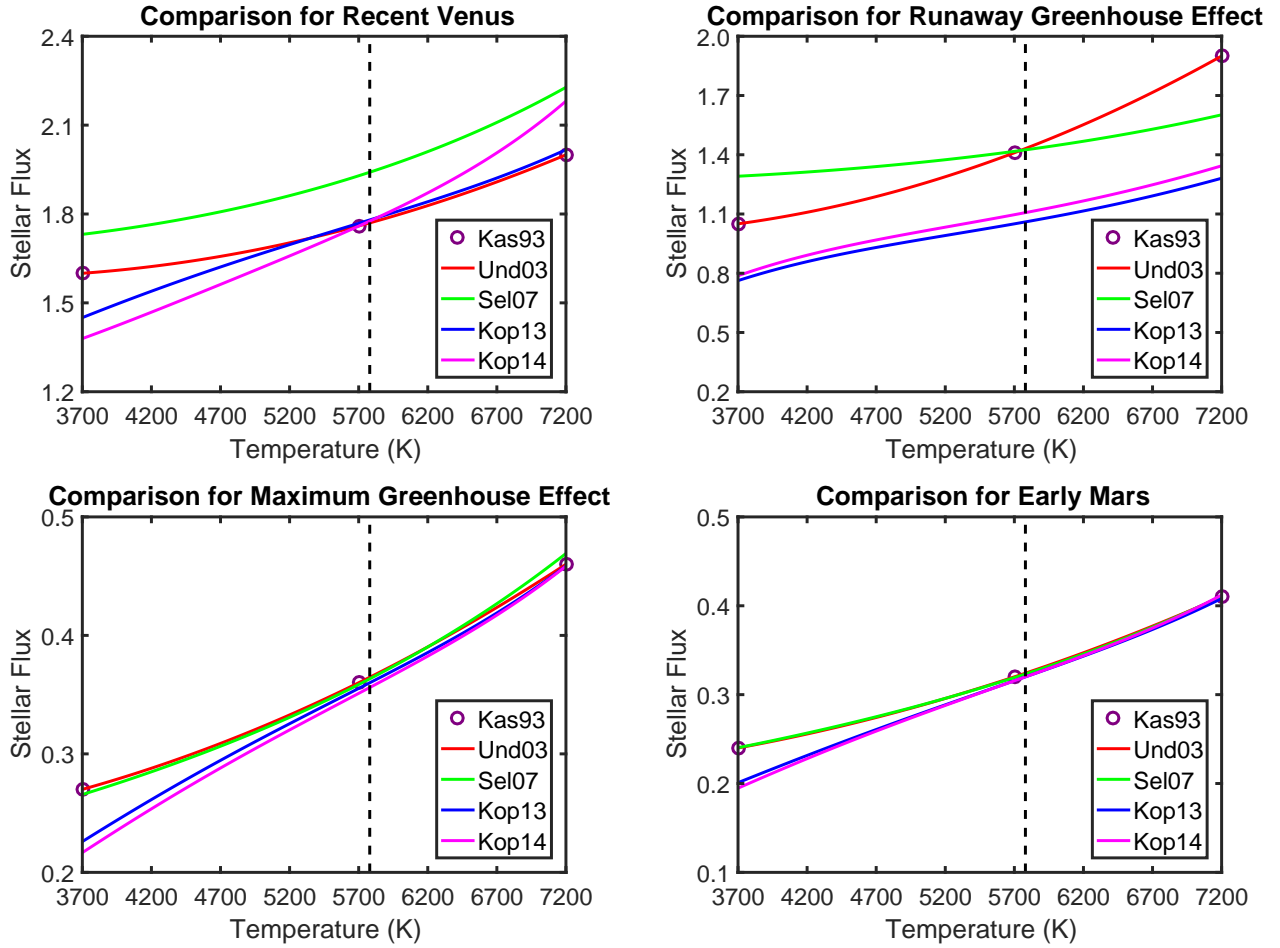


Fig. 2.— Comparison of effective stellar flux approximations from different works. Here the three circles indicate the stellar temperature data previously used by Kasting et al. (1993), whereas the dashed line depicts the now accepted value for the solar effective temperature given as 5777 K.

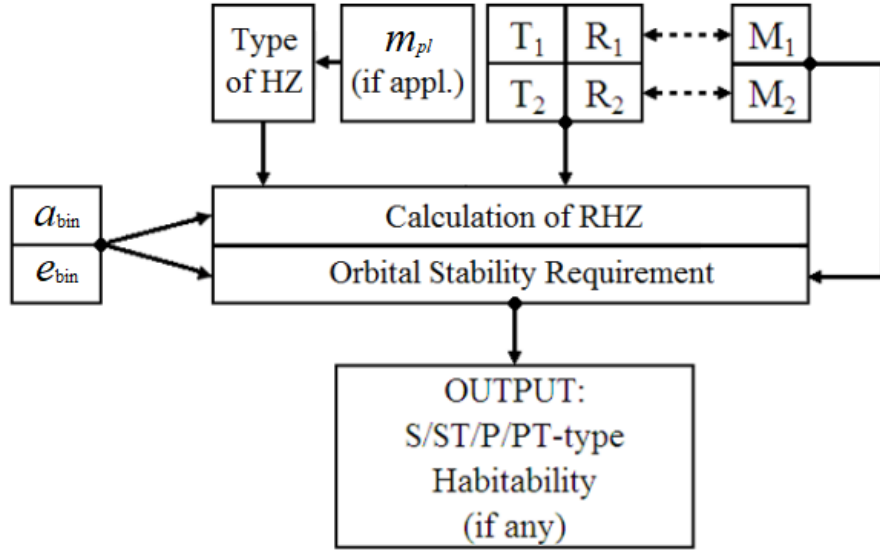


Fig. 3.— Flow diagram of BinHab 2.0 indicating the adopted method of solution. Feeds and the generation of the output are indicated by arrowed solid lines. For theoretical main-sequence stars, effective temperatures and stellar radii (T_i , R_i , with $i = 1, 2$), on the one hand, or stellar masses (M_i), on the other hand, may serve as input parameters, as indicated by double-headed dashed lines. See Cuntz & Bruntz (2014) for information on the original version of BinHab. An updated version of that tool has been deployed in 2018, largely developed by one of us (Zh. W.), which among other updates also takes into account the planetary mass m_{pl} .

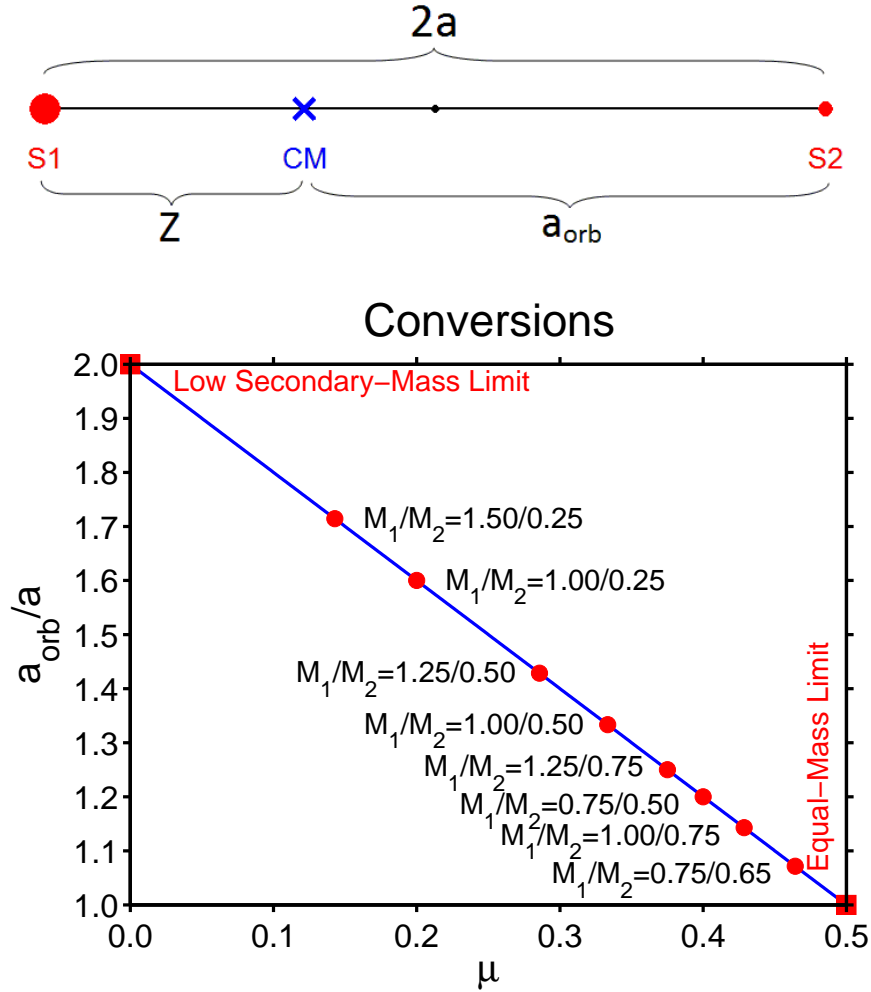


Fig. 4.— Coordinate system aimed at defining a_{orb} . Here S1 and S2 denote the two stellar components, which by default are of different masses. CM denotes the center of mass. Ratios a_{orb}/a for different mass ratios μ . The equal-mass limit $M_1 = M_2$ and the low secondary-mass limit $M_2/M_1 \rightarrow 0$ are conveyed for convenience.

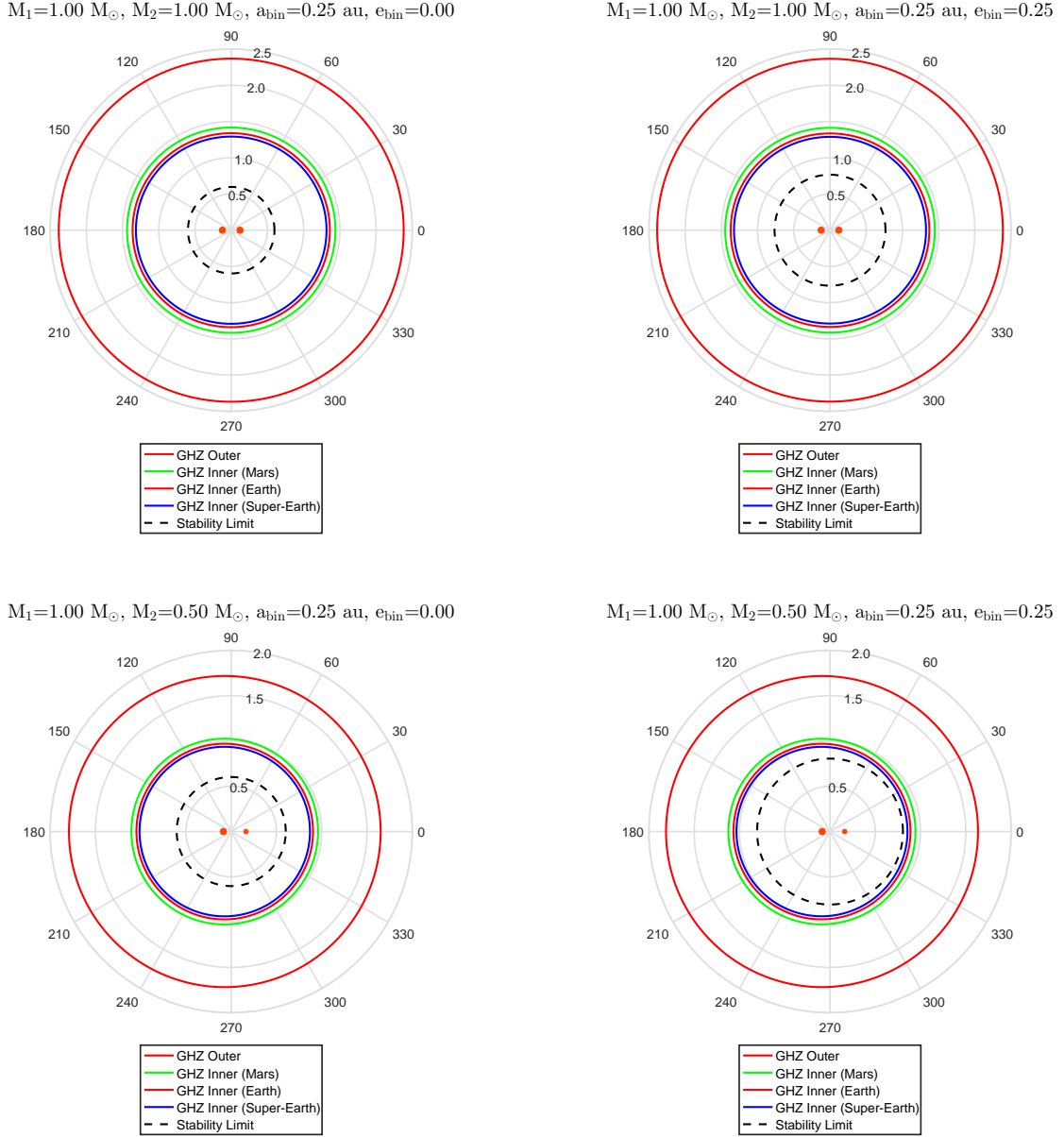
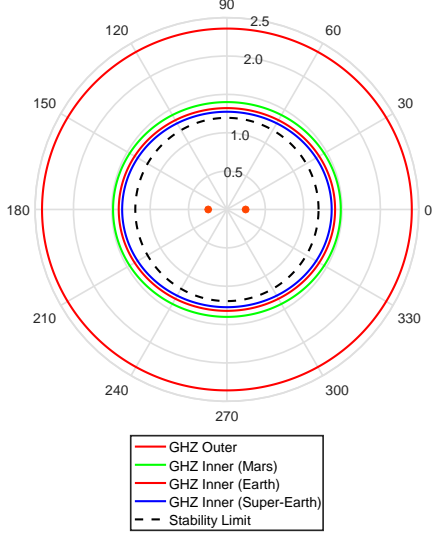
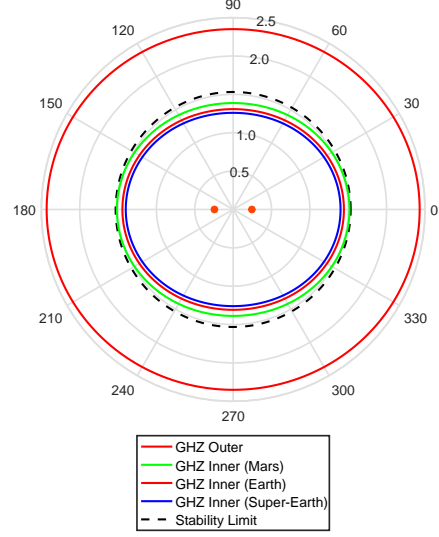


Fig. 5.— Polar diagrams for P -type habitable zones for the GHZ, assuming Mars-type ($0.1 M_\oplus$), Earth-type, and super-Earth-type ($5.0 M_\oplus$) planets, for two different combinations of stellar masses. The stability limit (which is an inner limit) is given as well. Here $a_{\text{bin}} = 0.25 \text{ au}$ is used. Results are shown for $e_{\text{bin}} = 0.00$ and 0.25 .

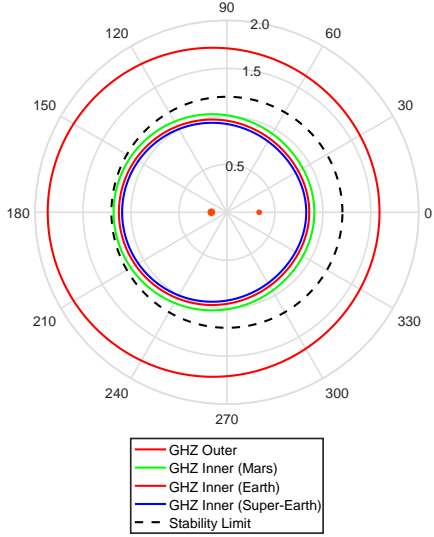
$M_1=1.00 M_\odot$, $M_2=1.00 M_\odot$, $a_{\text{bin}}=0.50$ au, $e_{\text{bin}}=0.00$



$M_1=1.00 M_\odot$, $M_2=1.00 M_\odot$, $a_{\text{bin}}=0.50$ au, $e_{\text{bin}}=0.25$



$M_1=1.00 M_\odot$, $M_2=0.50 M_\odot$, $a_{\text{bin}}=0.50$ au, $e_{\text{bin}}=0.00$



$M_1=1.00 M_\odot$, $M_2=0.50 M_\odot$, $a_{\text{bin}}=0.50$ au, $e_{\text{bin}}=0.25$

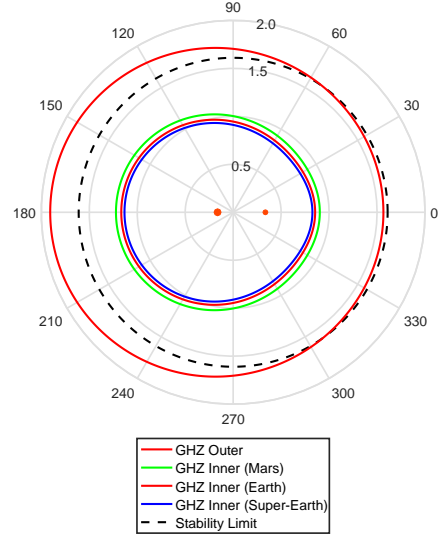


Fig. 6.— Same as Fig. 5, but with $a_{\text{bin}} = 0.50$ au.

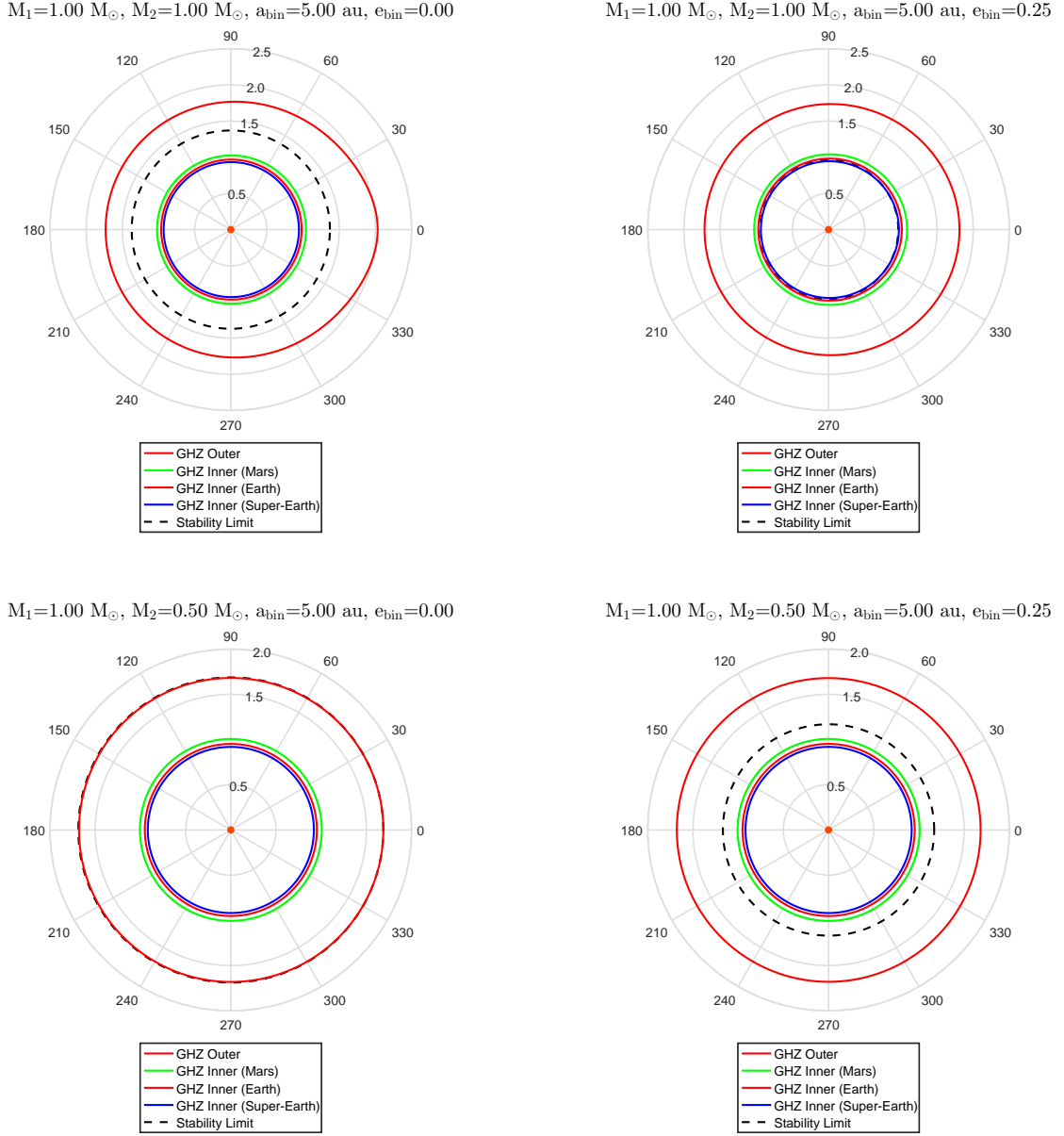


Fig. 7.— Polar diagrams for S -type habitable zones for the GHZ, assuming Mars-type ($0.1 M_{\oplus}$), Earth-type, and super-Earth-type ($5.0 M_{\oplus}$) planets, for two different combinations of stellar masses. The stability limit (which is an outer limit) is given as well. Here $a_{\text{bin}} = 5$ au is used. Results are shown for $e_{\text{bin}} = 0.00$ and 0.25 . The secondary star is assumed to be to the right. In the bottom figure (left), the lines for GHZ outer limit and planetary stability limit largely coincide.

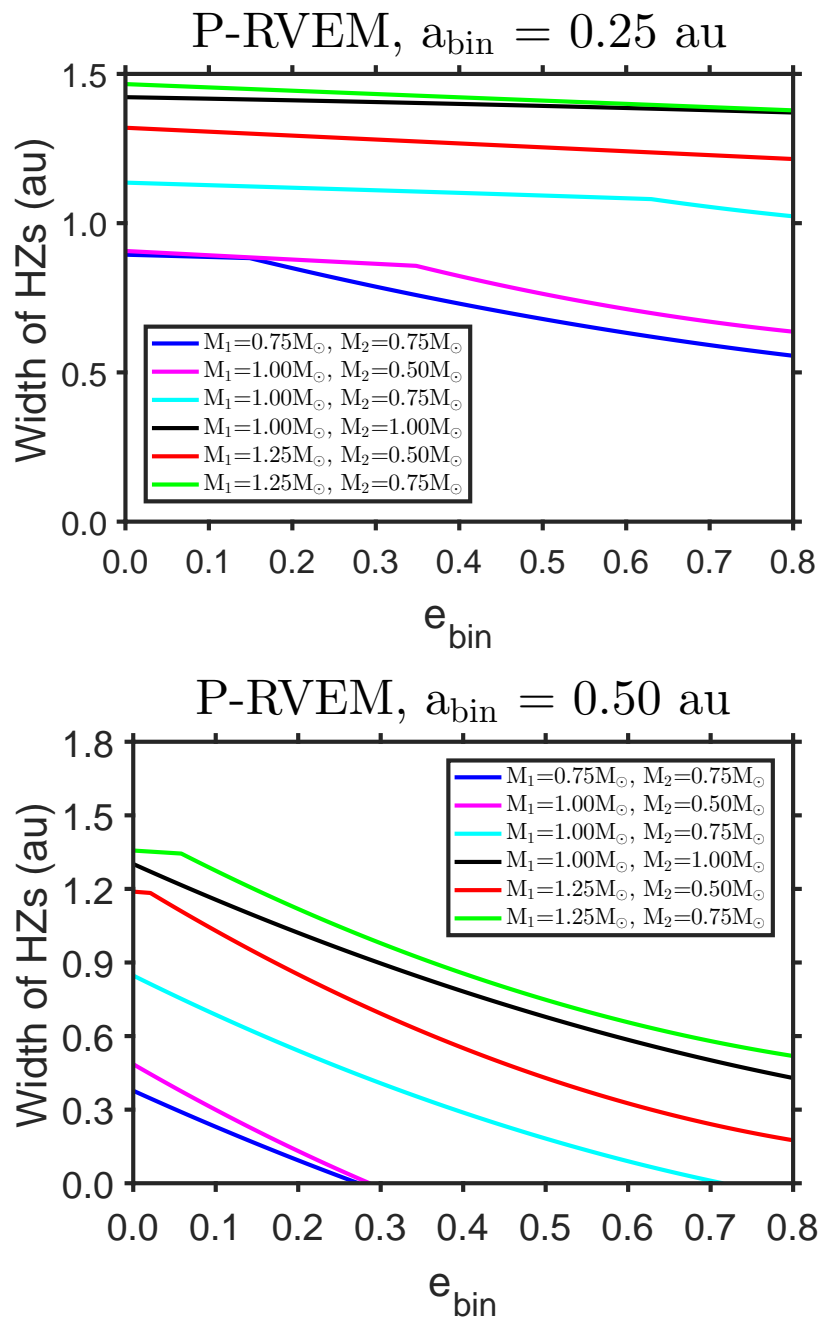


Fig. 8.— Widths of P/PT -type habitable zones based on RVEM limits for various binary systems. Here we depict results for $a_{\text{bin}} = 0.25$ au (top) and 0.50 au (bottom).

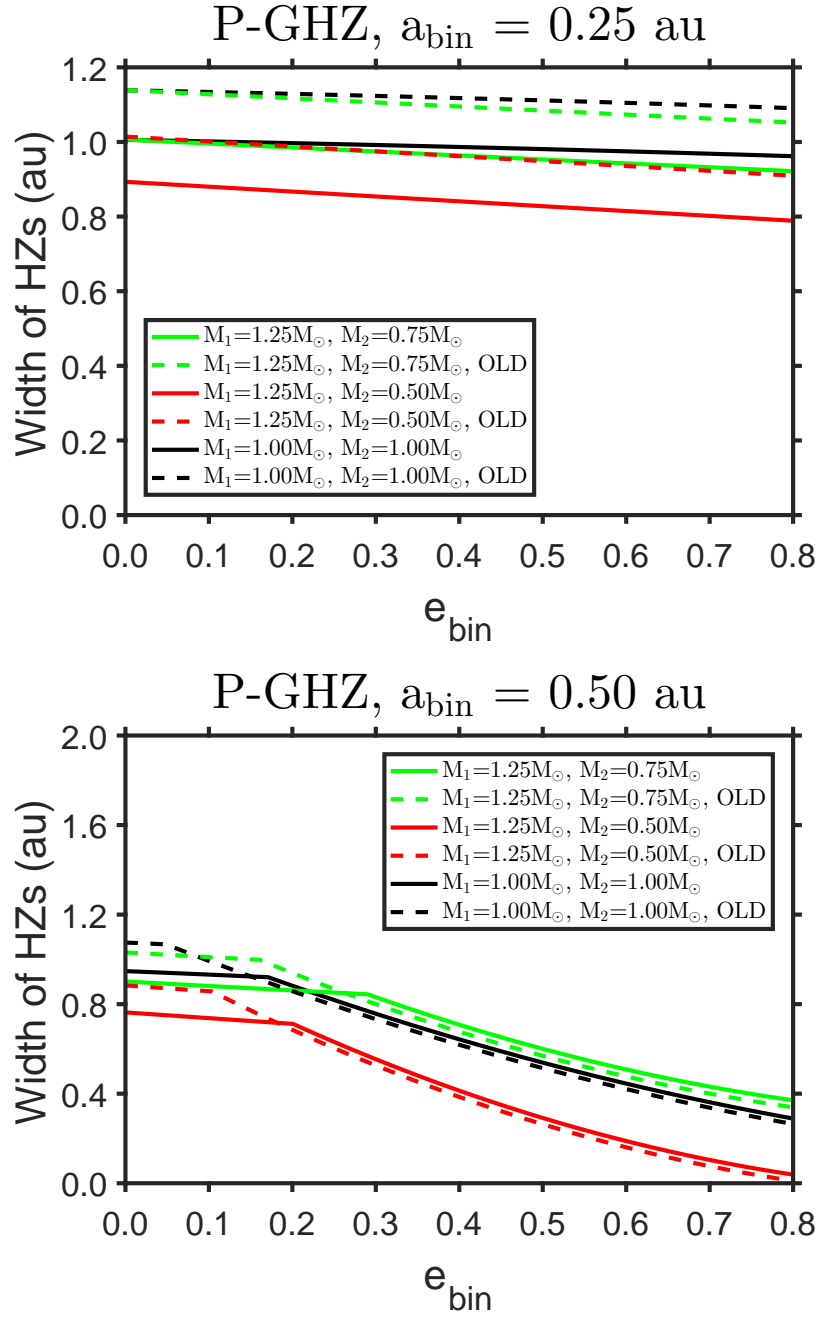


Fig. 9.— Widths of P/PT -type habitable zones based on GHZ limits, based on Earth-type planets, for various binary systems. Here we depict results for $a_{\text{bin}} = 0.25$ au (top) and 0.50 au (bottom). The models tagged as “OLD” are based on the effective stellar flux approximation by Selsis et al. (2007).

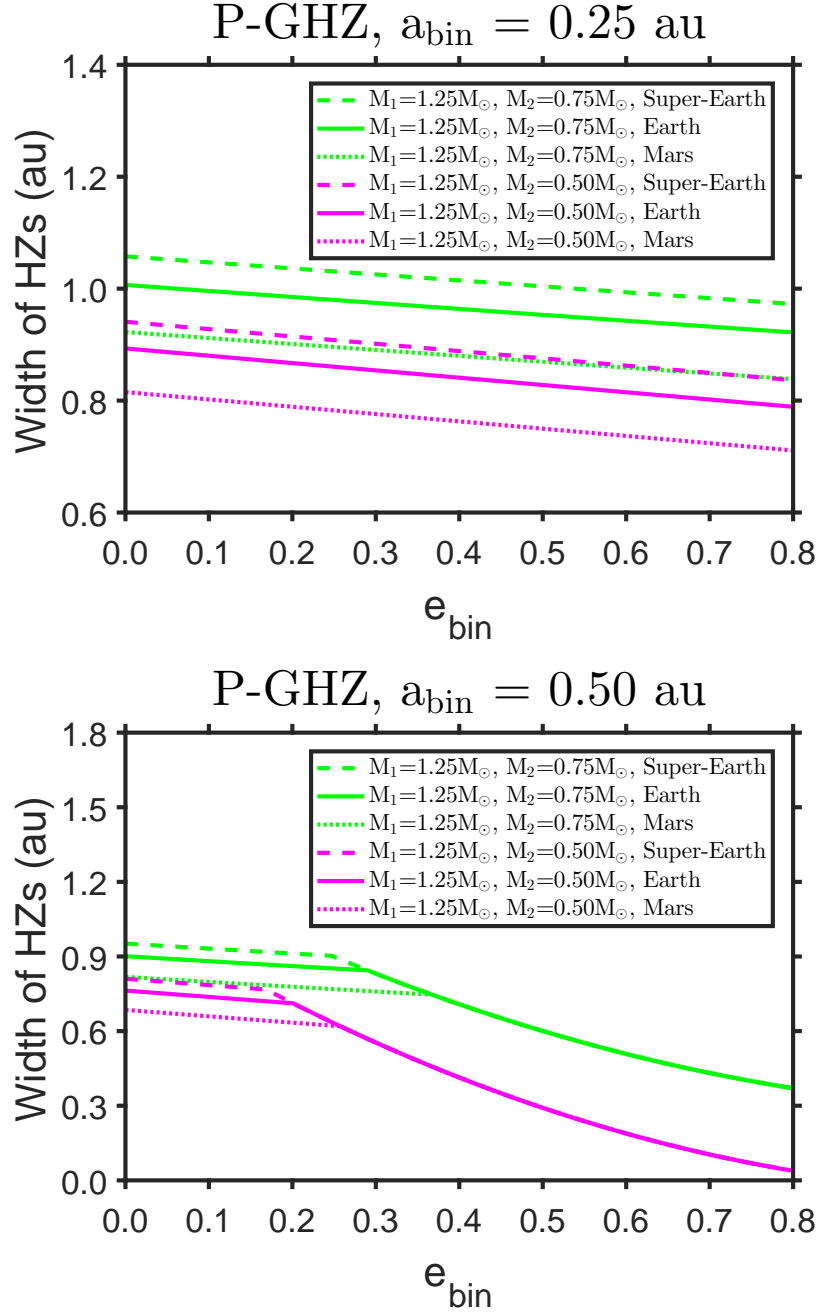


Fig. 10.— Widths of P/PT -type habitable zones based on GHZ limits, based on Mars-type ($0.1 M_\oplus$), Earth-type, and super-Earth-type ($5.0 M_\oplus$) planets, for various binary systems. Here we depict results for $a_{\text{bin}} = 0.25$ au (top) and 0.50 au (bottom).

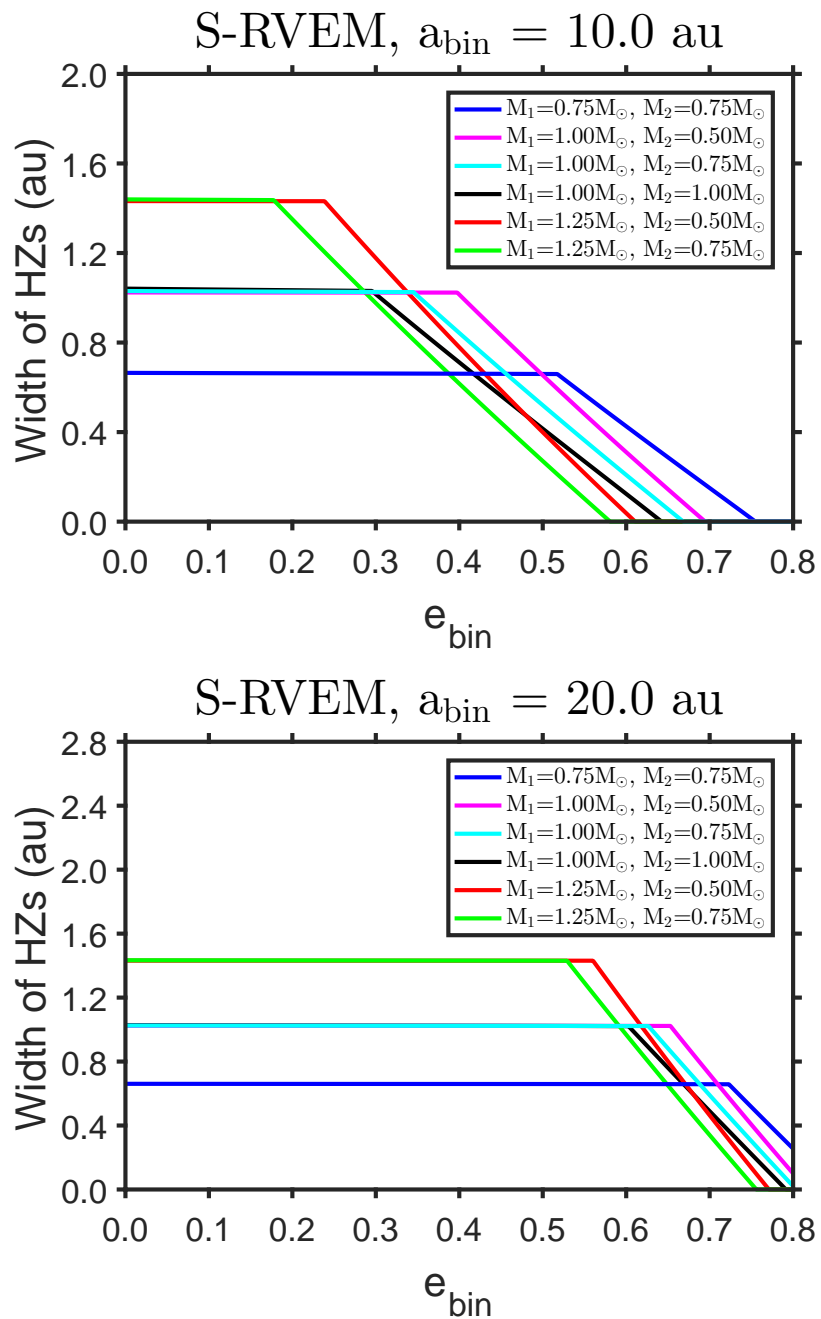


Fig. 11.— Widths of S/ST -type habitable zones based on RVEM limits for various binary systems. Here we depict results for $a_{\text{bin}} = 10$ au (top) and 20 au (bottom).

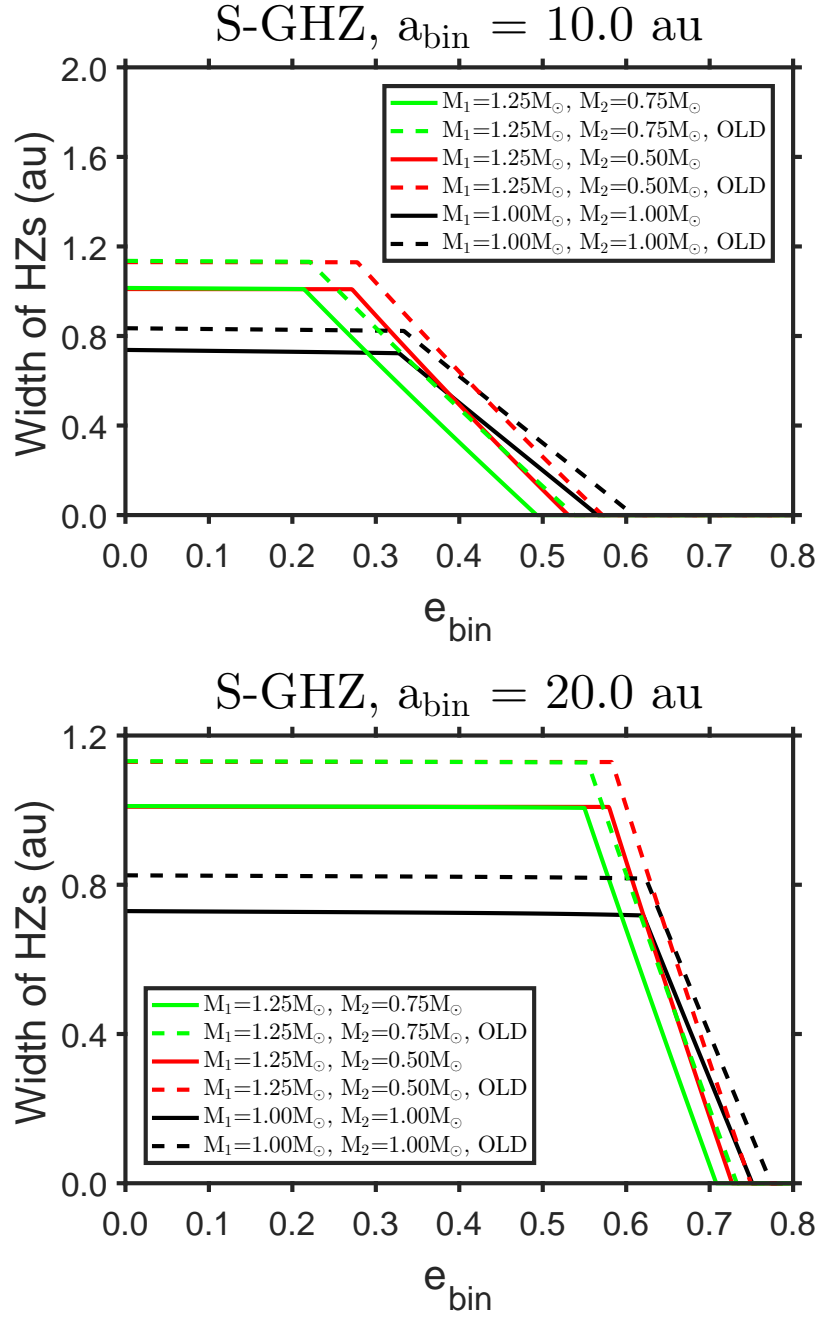


Fig. 12.— Widths of *S*/*ST*-type habitable zones based on GHZ limits, based on Earth-type planets, for various binary systems. Here we depict results for $a_{\text{bin}} = 10$ au (top) and 20 au (bottom). The models tagged as “OLD” are based on the effective stellar flux approximation by Selsis et al. (2007).

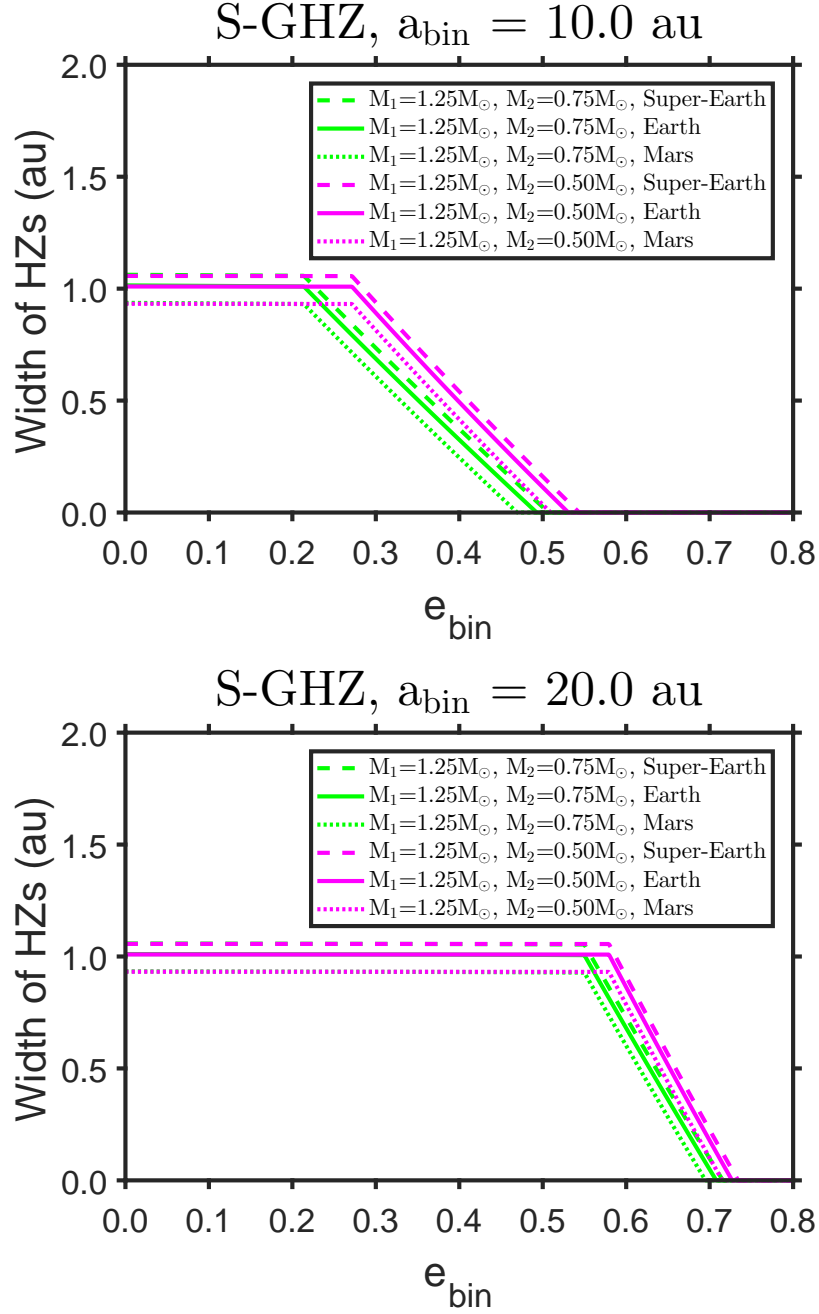


Fig. 13.— Widths of *S/ST*-type habitable zones based on GHZ limits, based on Mars-type ($0.1 M_{\oplus}$), Earth-type, and super-Earth-type ($5.0 M_{\oplus}$) planets, for various binary systems. Here we depict results for $a_{\text{bin}} = 10$ au (top) and 20 au (bottom).

Table 1. Stellar Parameters

Sp. Type	T_{eff}	R_*	L_*	M_*
...	(K)	(R_{\odot})	(L_{\odot})	(M_{\odot})
F0	7178	1.62	6.24	1.60
F2	6909	1.48	4.47	1.52
F5	6528	1.40	3.19	1.40
F8	6160	1.20	1.86	1.19
G0	5943	1.12	1.40	1.05
G2	5811	1.08	1.19	0.99
G2 (Sun)	5780	1.00	1.00	1.00
G5	5657	0.95	0.83	0.91
G8	5486	0.91	0.67	0.84
K0	5282	0.83	0.48	0.79
K2	5055	0.75	0.33	0.74
K4	4585	0.70	0.19	0.71
K5	4350	0.67	0.14	0.69
K6	4230	0.65	0.12	0.68
K8	4000	0.59	0.080	0.63
M0	3800	0.53	0.052	0.57
M1	3650	0.47	0.034	0.49
M2	3500	0.38	0.020	0.39

Table 2. Habitability Limits for the Sun, s_ℓ

Description	Indices		Models		
	ℓ	k	Kas93	Kop1314	
...	5700 K	5780 K	5780 K
...	(au)	(au)	(au)
Recent Venus	1	1	0.75	0.77	0.750
Runaway greenhouse effect	2	1	0.84	0.86	0.950
Runaway greenhouse effect	2	0	1.005
Runaway greenhouse effect	2	2	0.917
Moist greenhouse effect	3	1	0.95	0.97	0.993
Earth-equivalent position	0	1	0.993	$\equiv 1$	$\equiv 1$
First CO ₂ condensation	4	1	1.37	1.40	...
Maximum greenhouse effect, no clouds	5	1	1.67	1.71	1.676
Early Mars	6	1	1.77	1.81	1.768

Note. — Here 5700 K and 5780 K indicate the solar effective temperature adopted for the respective model calculation. The three-digit precision for some of the habitability limits are mostly conveyed for tutorial reasons. Moreover, the depictions for ℓ , indicating the inner / outer limits of the various types of HZs, do not always agree with those of Paper I and II. Furthermore, the index k indicates Mars-type ($0.1 M_\oplus$), Earth-type ($1.0 M_\oplus$), and super-Earth-type ($5.0 M_\oplus$) planets, corresponding to 0, 1, and 2, respectively.

Table 3. Types of Habitable Zones

Description	Kas93	Kop1314	Paper I & II	This work
Recent Venus	RVEM	GHZ	...	RVEM
Runaway greenhouse effect	GHZ	CHZ	EHZ, GHZ	GHZ
Moist greenhouse effect	CHZ	...	CHZ	...
First CO ₂ condensation	CHZ	...	CHZ	...
Maximum greenhouse effect, no clouds	GHZ	CHZ	GHZ	GHZ
Early Mars	RVEM	GHZ	...	RVEM
Maximum greenhouse effect, 100% clouds	EHZ	...

Note. — In each column, the double appearance of terms as, e.g., GHZ indicates either an inner or outer limit. See main text for definitions and background information.

Table 4. Main Target List

M_* (M_\odot)	Spectral Type ...	T_{eff} (K)	R_* (R_\odot)	L_* (L_\odot)	HZ(s_0) (au)
1.25	F8 V	6257	1.25	2.15	1.47
1.00	G2 V	5780	1.00	1.00	1.00
0.75	K2 V	5104	0.77	0.357	0.60
0.50	M1 V	3664	0.47	0.0359	0.19

Note. — HZ(s_0) are calculated as the Earth-equivalent distance.

Table 5. Habitability Classification for $M_1 = M_2 = 1.0 M_\odot$

e_{bin}	P	PT	ST	S
...	(au)	(au)	(au)	(au)
RVEM				
0.00	0.474	1.028	2.928	6.620
0.25	0.369	0.802	4.121	9.285
0.50	0.314	0.681	6.669	15.100
0.75	0.284	0.610	15.707	36.066
GHZ				
0.00	0.601	0.971	3.708	6.257
0.25	0.467	0.758	5.220	8.776
0.50	0.398	0.644	8.446	14.272
0.75	0.360	0.577	19.895	34.087

Note. — The values as obtained assume Earth-type planets. The second column indicates the maximum a_{bin} for P -type HZs to exist at a given binary eccentricity without the constraint of orbital stability. Values between the second and the third column indicate PT -type HZs to exist, i.e., the constraint of orbital stability applies. Values between the third and fourth column indicate that no HZs to exist. Values between the fourth and the fifth column indicate ST -type HZs to exist, i.e., the constraint of orbital stability applies. Values larger than those given in the fifth column indicate S -type HZs to exist, i.e., without the constraint of orbital stability.

Table 6. Habitability Classification for $M_1 = 1.25 M_\odot$, $M_2 = 0.75 M_\odot$

e_{bin}	P	PT	ST	S
...	(au)	(au)	(au)	(au)
RVEM				
0.00	0.542	1.076	3.398	7.825
0.25	0.407	0.817	4.870	11.219
0.50	0.346	0.691	8.038	18.562
0.75	0.317	0.626	19.365	44.921
GHZ				
0.00	0.687	1.016	4.304	7.397
0.25	0.516	0.772	6.168	10.606
0.50	0.438	0.653	10.180	17.547
0.75	0.401	0.592	24.528	42.466

Note. — See Table 5 for explanations.

Table 7. Critical Values of e_{bin} for P/PT -Type Habitability

Model	$a_{\text{bin}} = 0.25$ au				$a_{\text{bin}} = 0.50$ au			
	RVEM		GHZ		RVEM		GHZ	
Habitability Limits	P	PT	P	PT	P	PT	P	PT
M_1/M_2 (M_\odot/M_\odot)	P	PT	P	PT	P	PT	P	PT
1.25 / 1.25	†	†	†	†	0.318	†	†	†
1.25 / 1.00	†	†	†	†	0.150	†	0.474	†
1.25 / 0.75	†	†	†	†	0.058	†	0.290	†
1.25 / 0.50	†	†	†	†	0.020	†	0.200	†
1.00 / 1.00	†	†	†	†	...	†	0.171	†
1.00 / 0.75	0.630	†	†	†	...	0.714	0.019	0.569
1.00 / 0.50	0.348	†	†	†	...	0.286	...	0.221
0.75 / 0.75	0.148	†	0.477	†	...	0.272	...	0.202
0.75 / 0.50	...	†	0.137	0.763
0.50 / 0.50

Note. — (†) means that the critical value of e_{bin} is larger than 0.80; it could not be determined owing to the limitations of the work by HW99. Ellipsis indicates that there is no solution, which means no HZ could be found. The term “critical value” means that it is the *maximal* possible value for e_{bin} , allowing P -type or PT -type habitability to exist. The results are given for Earth-type planets.

Table 8. Critical Values of e_{bin} for P -Type Habitability, cont'd

Model	$a_{\text{bin}} = 0.25$ au			$a_{\text{bin}} = 0.50$ au		
	M_1/M_2 (M_\odot/M_\odot)	Mars	Earth	Super-Earth	Mars	Earth
1.25 / 1.25	†	†	†	†	†	0.722
1.25 / 1.00	†	†	†	0.596	0.474	0.410
1.25 / 0.75	†	†	†	0.367	0.290	0.247
1.25 / 0.50	†	†	†	0.257	0.200	0.168
1.00 / 1.00	†	†	†	0.235	0.171	0.133
1.00 / 0.75	†	†	†	0.063	0.019	...
1.00 / 0.50	†	†	†
0.75 / 0.75	0.596	0.477	0.414
0.75 / 0.50	0.194	0.137	0.105
0.50 / 0.50

Note. — Same as Table 7, but for Mars-type ($0.1 M_\oplus$), Earth-type, and super-Earth-type ($5.0 M_\oplus$) planets.

Table 9. Critical Values of e_{bin} for S/ST -Type Habitability

Model	$a_{\text{bin}} = 10.0$ au				$a_{\text{bin}} = 20.0$ au			
Habitability Limits	RVEM		GHZ		RVEM		GHZ	
M_1/M_2 (M_\odot/M_\odot)	S	ST	S	ST	S	ST	S	ST
1.25 / 1.25	0.057	0.520	0.101	0.415	0.473	0.727	0.497	0.670
1.25 / 1.00	0.118	0.551	0.157	0.454	0.500	0.741	0.522	0.689
1.25 / 0.75	0.177	0.580	0.213	0.492	0.529	0.755	0.549	0.707
1.25 / 0.50	0.238	0.610	0.271	0.530	0.560	0.771	0.579	0.726
1.00 / 1.00	0.295	0.642	0.327	0.565	0.602	0.791	0.620	0.751
1.00 / 0.75	0.345	0.668	0.374	0.599	0.626	†	0.642	0.766
1.00 / 0.50	0.397	0.694	0.424	0.632	0.652	†	0.667	0.783
0.75 / 0.75	0.517	0.754	0.539	0.705	0.723	†	0.734	†
0.75 / 0.50	0.558	0.776	0.578	0.733	0.743	†	0.754	†
0.50 / 0.50	0.785	†	0.794	†	†	†	†	†

Note. — (†) means that the critical value of e_{bin} is larger than 0.80; it could not be determined owing to the limitations of the work by HW99. Ellipsis indicates that there is no solution, which means no HZ could be found. The term “critical value” means that it is the *maximal* possible value for e_{bin} , allowing S -type or ST -type habitability to exist. The results are given for Earth-type planets.

Table 10. Critical Values of e_{bin} for *ST*-Type Habitability, cont'd

Model	$a_{\text{bin}} = 10.0$ au			$a_{\text{bin}} = 20.0$ au		
	M_1/M_2 (M_\odot/M_\odot)	Mars	Earth	Super-Earth	Mars	Earth
1.25 / 1.25	0.387	0.415	0.432	0.655	0.670	0.680
1.25 / 1.00	0.429	0.454	0.470	0.675	0.689	0.697
1.25 / 0.75	0.469	0.492	0.507	0.695	0.707	0.715
1.25 / 0.50	0.509	0.530	0.543	0.715	0.726	0.734
1.00 / 1.00	0.545	0.565	0.578	0.740	0.751	0.757
1.00 / 0.75	0.580	0.599	0.610	0.756	0.766	0.772
1.00 / 0.50	0.616	0.632	0.642	0.774	0.783	0.788
0.75 / 0.75	0.691	0.705	0.713	†	†	†
0.75 / 0.50	0.721	0.733	0.740	†	†	†
0.50 / 0.50	†	†	†	†	†	†

Note. — Same as Table 9, but for Mars-type ($0.1 M_\oplus$), Earth-type, and super-Earth-type ($5.0 M_\oplus$) planets.

Table 11. Stellar Parameter Comparison

Model	Sp. Type	M	T_{eff}	R_*	L_*
...	...	(M_{\odot})	(K)	(R_{\odot})	(L_{\odot})
Mann et al. (2013)	\sim M5 V	0.2	3292	0.233	5.727×10^{-3}
Baraffe et al. (2015)	\sim M5 V	0.2	3262	0.218	4.786×10^{-3}

Table 12. Equal Mass Systems: $M_1 = M_2 = 0.20 M_\odot$

Habitable Zone	a_{bin}	e_{bin}	Stellar Model			
			Mann et al. (2013)		Baraffe et al. (2015)	
			Inner Limit	Outer Limit	Inner Limit	Outer Limit
	(au)		(au)	(au)	(au)	(au)
<i>P</i> -type GHZ	0.01	0.00	0.1115	0.2180	0.1020	0.1996
<i>P</i> -type GHZ	0.01	0.40	0.1118	0.2180	0.1024	0.1996
<i>P</i> -type GHZ	0.05	0.00	0.1188	0.2166	0.1099	0.1981
<i>P</i> -type GHZ	0.05	0.40	0.1252	0.2153	0.1166	0.1966
<i>S</i> -type GHZ	2.50	0.00	0.0786	0.1545	0.0719	0.1414
<i>S</i> -type GHZ	2.50	0.40	0.0787	0.1543	0.0720	0.1413
<i>S</i> -type GHZ	5.00	0.00	0.0786	0.1543	0.0719	0.1413
<i>S</i> -type GHZ	5.00	0.40	0.0786	0.1542	0.0719	0.1412

Note. — Here the RHZ limits are listed for different systems. The *P*-type limits are given from the mass center of the binary star system, whereas the *S*-type limits are given from the center of the primary. Results are given for the GHZ based on the work by Kopparapu et al. (2013, 2014), assuming a planet of one Earth mass. The high precision for the data has been given for mostly tutorial reasons. Baraffe et al. (2015) present M-star models of different ages. Here we assume 5 Gyr, a data that is highly inconsequential.

Table 13. Non-Equal Mass Systems: $M_1 = 1.00 M_\odot$, $M_2 = 0.20 M_\odot$

Habitable Zone	a_{bin}	e_{bin}	Stellar Model			
			Mann et al. (2013)		Baraffe et al. (2015)	
			Inner Limit	Outer Limit	Inner Limit	Outer Limit
	(au)	(au)	(au)	(au)	(au)	
<i>P</i> -type GHZ	0.01	0.00	0.9553	1.6815	0.9548	1.6803
<i>P</i> -type GHZ	0.01	0.40	0.9559	1.6809	0.9554	1.6797
<i>P</i> -type GHZ	0.05	0.00	0.9617	1.6752	0.9612	1.6740
<i>P</i> -type GHZ	0.05	0.40	0.9649	1.6720	0.9645	1.6708
<i>S</i> -type GHZ	5.00	0.00	0.9506	1.6765	0.9506	1.6764
<i>S</i> -type GHZ	5.00	0.40	0.9511	1.6763	0.9510	1.6762
<i>S</i> -type GHZ	6.00	0.00	0.9506	1.6763	0.9505	1.6763
<i>S</i> -type GHZ	6.00	0.40	0.9509	1.6762	0.9508	1.6762

Note. — See Table 12 for comments.